TUDelft

Delft University of Technology

A coupled model of transport-reaction-mechanics with trapping. Part I – Small strain analysis

Salvadori, A.; McMeeking, R.; Grazioli, D.; Magri, M.

Important note
To cite this publication, please use the final published version (if applicable).
Please check the document version above.

A coupled model of transport-reaction-mechanics with trapping. Part I - small strain analysis.

Salvadori A.[1,2], McMeeking R.[3,4,5], Grazioli D.[1,6], Magri M.[1]

[1] DICATAM - Dipartimento di Ingegneria Civile, Architettura, Territorio, Ambiente e di Matematica
Università di Brescia, via Branze 43, 25123 Brescia, Italy

[2] Department of Aerospace and Mechanical Engineering,
Center for Shock Wave-processing of Advanced Reactive Materials,
University of Notre Dame, Notre Dame, Indiana.

[3] Materials and Mechanical Engineering Departments, University of California,
Santa Barbara CA 93106, USA

[4] School of Engineering, University of Aberdeen, King's College, Aberdeen AB24 3UE, UK

[5] Leibniz Institute for New Materials, Campus D2 2, Saarbruecken, Germany

[6] Faculty of Civil Engineering and Geosciences, Delft University of Technology,
P.O. Box 5048, 2600 GA Delft, The Netherlands

February 21, 2018

Abstract

A fully coupled model for mass and heat transport, mechanics, and chemical reactions with trapping is proposed. It is rooted in non-equilibrium rational thermodynamics and assumes that displacements and strains are small. Balance laws for mass, linear and angular momentum, energy, and entropy are stated. Thermodynamic restrictions are identified, based on an additive strain decomposition and on the definition of the Helmholtz free energy. Constitutive theory and chemical kinetics are studied in order to finally write the governing equations for the multi-physics problem. The field equations are solved numerically with the finite element method, stemming from a three-fields variational formulation. Three case-studies on vacancies redistribution in metals, hydrogen embrittlement, and the charge-discharge of active particles in Li-ion batteries demonstrate the features and the potential of the proposed model.

1 Introduction

Several multi-disciplinary applications involve mass transport - driven by diffusion, migration or both - coupled with chemo-thermo-mechanics. In many cases, only a fraction of the total available mass of mobile species is effectively transported, whereas a significant counterpart remains immobilized by specific phenomena occuring concurrently with transport, i.e. trapping. Some examples clarify this concept.

One example is when metals are exposed to hydrogen gas, typically in storage tanks, and H atoms diffuse within the crystalline structure of the metal [1, 2, 3, 4, 5, 6, 7, 8]. H is found then not only in interstitial lattice sites, but also in defects such as vacancies, dislocations, grain boundaries, second-phase particle boundaries, and voids. Since such trapping of H in defects is energetically favorable, the mean residence time of diffusing hydrogen atoms is significantly longer in defects than in interstitial lattice sites. Furthermore, hydrogen free defects are filled very rapidly.

In electrochemical energy storage the fundamental mechanism of charge-discharge is the motion of ions between two electrodes. Particularly in Li-ion batteries, insertion of ions in active particles often alters the crystal structure of the particle itself, leading to a core-shell configuration with one segment, e.g. the shell in the case of insertion, rich in lithium with a sharp interface that separates it from a pristine inner core [9, 10, 11, 12, 13, 14]. Formation of chemical bonds between guest and host atoms allows alloying of lithium ions with the host matrix, transforming its initial crystal structure. Either fully reversible or not upon

delithiation, those chemical reactions immobilize lithium ions, i.e. trap them, and make them unavailable for further diffusion in the storage particle.

A third example is where cells interact with extra-cellular matrix (ECM) proteins via focal adhesions, creating multi-molecular complexes. Focal adhesions consist of complex plaques of several proteins, but integrins are one of the most significant molecules within adhesions as they provide the trans-membrane connection of the cell to the ECM via extracellular domains that bind to external ligands. Integrins exist in two conformational states, the so-called low- and high-affinity configurations (with respect to extra cellular ligands): only the high-affinity integrins interact with and bond to the extra-cellular matrix and become immobilized, i.e. trapped, whereas the low affinity ones remain mobile on the bilipid membrane. The relationship between the rate of the kinetics of transformation between the high-affinity and low affinity states and the diffusion speed of the integrin across the lipid bilayer membrane is fundamental to the focal adhesion process and contributes to their characteristics in terms of location in the cell membrane and shape and size [15, 16, 17, 18].

We note that in addition to the 3 examples described above, vacancies in metals, dendritic growth, solid propellant, bio-electrochemistry, solute solidification, and moisture diffusion in polymer nanocomposites provide additional examples of diffusion with trapping.

We do not model interface trap phenomena explicitly as was done by Torquato [19], as we use the *network* model of Larche and Cahn [20] instead. Thus it is assumed that the lattice sites of the hosting material form a network within which guest atoms can diffuse. In contrast, trap sites are taken to be isolated from one another and, hence, trapped atoms are immobilized within their specific trap. As noted above, trapped species are often associated with a separation of phases with interphase thickness controlled by material parameters that determine the degree of interaction among species. Reaction dominated processes favor sharp interphases, as will be seen in the numerical applications below, whereas diffusion controlled regimes are characterized by smooth, diffuse phase transitions. Our formulation and the solution of the associated boundary value problems allow both possibilities to arise.

Trapping of guest atoms is a kinetic process involving chemical and physical reactions described by the mass action law, set in a well-established thermodynamic framework [21, 22]. Deviation from stoichiometry in a solid composition can occur due to diffusion, and alloying reactions may cause large degrees of swelling that, when constrained, lead to mechanical stress. Such mechanical effects influence all other processes, since all chemo-transport-thermo-mechanical processes are coupled. These interactions are accounted for in this paper, within a rigorous thermodynamic setting [23, 24] in the simple framework of small strains. Extension to large strain will follow in future work. Elastic and swelling contributions through such coupling suggest some modifications to the law of mass action in its classical form, thus extending the *van't Hoff* relation [25] to the case of trapping.

The paper is organized as follows. Balance equations for conservation of mass, linear and angular momentum, energy, and entropy are introduced in sections 2 and 3. Thermodynamic restrictions arise as usual from the Curie symmetry principle and from the Coleman-Noll procedure. Subsequently in section 4 constitutive theory provides consistent phenomenological specifications for heat and mass fluxes, mechanical stress, as well as for the evolution of inelastic processes. Coupling of chemical kinetics to all other processes is analyzed in section 5, pinpointing when phenomena can be categorized as not rate limiting and therefore modeled as infinitely fast. Governing equations are summarized and subsequently written in weak form in the so-called *three-fields formulation*, treating pressure as an independent variable not constitutively characterized. Three case studies are investigated in order of increasing complexity: the first concerns the redistribution of vacancies in an aluminum lattice, induced by a stress field; the second studies the effect of stress and trapping on hydrogen distribution in a plastically deforming steel; the last describes the insertion, diffusion, and trapping of lithium in active particles within a battery. The influence of material parameters on the evolution of processes is highlighted.

2   Balance laws

Most species transport models consider the effect of hydrostatic stress and trapping on the species distribution in an inelastically deforming hosting material, assuming that species diffuse through lattice sites and that trap

sites are filled via species diffusion. Only saturable and reversible traps are considered, such as dislocation cores. They are assumed to be isolated, in the sense that they do not form an extended network, and so do not present a continuous path for lattice diffusion. For this reason, some of the species flowing across the boundary $\partial \mathcal{P}$ of any subpart $\mathcal{P}$ of the body under investigation enters traps in the bulk and thus cease to contribute to species transport. The flux of species $\vec{h}$ is assumed to be purely interstitial lattice diffusion (and termed $\vec{h}_L$ from now on[1]), following Larchè and Cahn [20, 26].

In the realm of small displacements and strains, there is no need to distinguish between material and spatial time derivative. When dealing with composite functions of the form $\phi(a(z), z)$ we will identify the *total* derivative with the roman symbol d and the *partial* derivative with the symbol ∂. It thus holds:

$$\frac{\mathrm{d}}{\mathrm{d}\,z}\phi(a(z), z) = \frac{\partial \phi}{\partial\,a}\frac{\mathrm{d}\,a}{\mathrm{d}\,z} + \frac{\partial \phi}{\partial\,z}$$

This notation will be used in the time derivative of internal and Helmholtz free energies, and of entropy. It will be also used in section 3.6 in dealing with a composite form of the internal energy.

2.1 Mass balance

The trapping process of a generic species, denoted henceforth with H, is described as a chemical reaction,

$$\mathrm{H}_L \underset{k_L}{\overset{k_T}{\rightleftarrows}} \mathrm{H}_T \ , \tag{1}$$

which portrays the conversion of mobile to trapped species and vice-versa by the rate of the reaction (1), denoted with $w^{(1)}$. Reaction (1) is unbalanced during species diffusion and interstitial species H_L is either made available or trapped. The mass balance equations yield:

$$\frac{\partial c_L}{\partial t} + \mathrm{div}\left[\vec{h}_L\right] + w^{(1)} = s_L \ , \tag{2a}$$

$$\frac{\partial c_T}{\partial t} - w^{(1)} = s_T \ . \tag{2b}$$

Symbols in equations (2) have the following meaning: c_β (with $\beta = L, T$) is the *molarity* (i.e. the number of moles per unit volume) of a generic species H_β; t is time; $\vec{h}_\beta$ is the mass flux in terms of moles, i.e. the number of moles of species H_β measured per unit area per unit time; s_L is the rate in moles per unit volume per unit time at which lattice species is generated by sources, and s_T is that for trapped species. Concentrations c_β are defined in space and time, i.e. $c_\beta = c_\beta(\vec{x}, t)$. The same holds for $\vec{h}_L$, $w^{(1)}$, s_β. Functional dependence however is specified when necessary only, to favor readability. It is assumed that trapped species are immobile since traps are isolated. Therefore, a mass flux term is absent in Eq. (2b).

2.2 Balance of momentum

The usual balance of forces:
$$\mathrm{div}\left[\boldsymbol{\sigma}\right] + \vec{b} = \vec{0} \tag{3}$$

holds, where $\boldsymbol{\sigma}$ is the Cauchy stress tensor, $\vec{b}$ is the body force per unit volume, and we have assumed inertia forces to be negligible. The symmetry of the stress tensor follows from the balance of angular momentum [23].

2.3 Weak form and boundary conditions

The weak formulation of balance equations (2, 3) results from multiplication by a suitable set of test functions - here denoted with a superposed carat - and from an integration upon the domain, exploiting Green's formula to reduce the order of differentiation. Consider the mass balance Eq.(2-a):

$$\int_V \hat{\mu}_L \ \left\{\frac{\partial c_L}{\partial t} + \mathrm{div}\left[\vec{h}_L\right] + w^{(1)} - s_L\right\} \mathrm{d}V = \tag{4}$$

---

[1]Henceforth the subscript L refers to lattice (interstitial) sites and the subscript T to trap sites.

$$= \int_V \hat{\mu}_L \, \frac{\partial c_L}{\partial t} \, \mathrm{d}V + \int_V \mathrm{div}\left[\hat{\mu}_L \, \vec{h}_L\right] - \nabla\left[\hat{\mu}_L\right] \cdot \vec{h}_L \, \mathrm{d}V + \int_V \hat{\mu}_L \, (w^{(1)} - s_L) \, \mathrm{d}V$$

$$= \int_V \hat{\mu}_L \, \frac{\partial c_L}{\partial t} \, \mathrm{d}V - \int_V \nabla\left[\hat{\mu}_L\right] \cdot \vec{h}_L \, \mathrm{d}V + \int_V \hat{\mu}_L \, (w^{(1)} - s_L) \, \mathrm{d}V + \int_{\partial V} \hat{\mu}_L \, \vec{h}_L \cdot \vec{n} \, \mathrm{d}\Gamma = 0 \ .$$

Within (4) a contribution is defined on the boundary ∂V, which has outward unit normal $\vec{n}$. It is unusual to know a priori the mass flux through the boundary. It is rather more natural to impose thermodynamic equilibrium between external and internal species at the domain boundary[2]. Nevertheless, for the sake of completeness, boundary conditions will be written as

$$\vec{h}_L \cdot \vec{n} = \overline{h} \qquad \vec{x} \in \partial^N V \ . \tag{5a}$$

The weak form of Eq. (2b) can be derived simply as:

$$\int_V \hat{\mu}_T \left\{ \frac{\partial c_T}{\partial t} - w^{(1)} - s_T \right\} \mathrm{d}V = 0 \ . \tag{6}$$

Finally, for the equilibrium equations (3) one writes the principle of virtual work as

$$\int_V -\hat{\varepsilon} : \boldsymbol{\sigma} + \vec{\hat{u}} \cdot \vec{b} \, \mathrm{d}V + \int_{\partial V} \vec{\hat{u}} \cdot \boldsymbol{\sigma} \cdot \vec{n} \, \mathrm{d}\Gamma = 0 \ . \tag{7}$$

The given tractions along the Neumann part of the boundary $\partial^N V$ will be denoted with $\vec{\overline{p}}$

$$\boldsymbol{\sigma} \cdot \vec{n} = \vec{\overline{p}} \qquad \vec{x} \in \partial^N V \ . \tag{8}$$

A Dirichlet boundary condition (usually homogeneous) for the displacements is added along the Dirichlet part $\partial^D V$.

In conclusion, the weak form of the balance equations can be written in the time interval $[0, t_f]$ as

$$\text{Find } y \in \mathcal{V}^{[0,t_f]} \text{ such that} \qquad \frac{\partial}{\partial t} b\left(\hat{y}, z(t)\right) + a(\hat{y}, y(t)) = f(\hat{y}) \qquad \forall \hat{y} \in \mathcal{V} \tag{9}$$

where

$$b\left(\hat{y}, z\right) = \int_V \hat{\mu}_L \, c_L + \hat{\mu}_T \, c_T \, \mathrm{d}V \ ,$$

$$a\left(\hat{y}, y\right) = -\int_V \nabla\left[\hat{\mu}_L\right] \cdot \vec{h}_L \, \mathrm{d}V + \int_V \hat{\varepsilon} : \boldsymbol{\sigma} \, \mathrm{d}V + \int_V (\hat{\mu}_L - \hat{\mu}_T) \, w^{(1)} \, \mathrm{d}V \ ,$$

$$f\left(\hat{y}\right) = -\int_{\partial^N V} \hat{\mu}_L \, \overline{h} \, \mathrm{d}\Gamma + \int_{\partial^N V} \vec{\hat{u}} \cdot \vec{\overline{p}} \, \mathrm{d}\Gamma + \int_V \vec{\hat{u}} \cdot \vec{b} \, \mathrm{d}V + \int_V \hat{\mu}_L \, s_L + \hat{\mu}_T \, s_T \, \mathrm{d}V \ ,$$

with $z = \{c_L, c_T\}$, $y = \{\mu_L, \mu_T, \vec{u}\}$. Columns z and y collect the time-dependent unknown fields. Column $\hat{y}$ collects the steady-state test functions that correspond to the unknown fields in y.

To computationally solve the (either weak or strong) problem, constitutive equations must be specified, which is the subject of section 3. Ellipticity of the operators, functional and numerical properties of the solution and of its approximation depend on the constitutive assumptions and on the choice of the correct functional spaces $\mathcal{V}^{[0,t_f]}, \mathcal{V}$. However the identification of these spaces falls beyond the scope of the present paper.

The weak form (9) acquires the usual physical meaning of power expenditure: for this reason the selection of the shape functions has been made in terms of chemical potentials $\hat{\mu}$ rather than concentrations.

---

[2]See also section 7 to this aim. Note that the extent of Neumann boundaries are defined for each field and differ from field to field. In order to enlighten the notation however the field dependence has not been specified in writing $\partial^N V$ and has been left implicit. The same arguments apply to Dirichlet boundaries.

3 Thermodynamics

3.1 Energy balance

Denote with $\mathcal{B} \in \mathbb{R}^3$ the spatial domain of problem (2, 3). Consider an arbitrary material region $\mathcal{P} \subset \mathcal{B}$, which is taken as non-convecting. The first law of thermodynamics represents the balance of the interplay among the internal energy of $\mathcal{P}$, the power expended on $\mathcal{P}$, the heat transferred in $\mathcal{P}$, and the power due to mass exchanged on $\mathcal{P}$. The energy balance for the problem at hand, using the notation introduced in the former section for *quasi-static interactions*, reads:

$$\frac{\mathrm{d}\mathcal{U}}{\mathrm{d}t}(\mathcal{P}) = \mathcal{W}_u(\mathcal{P}) + \mathcal{Q}_u(\mathcal{P}) + \mathcal{T}_u(\mathcal{P}) \,, \tag{10}$$

with $\mathcal{U}$ the net internal energy of $\mathcal{P}$, $\mathcal{W}_u$ the mechanical external power, $\mathcal{Q}_u$ the power due to heat transfer, $\mathcal{T}_u$ the power due to mass transfer[3]. It is assumed that each of these processes is *energetically separable* in the balance. The individual contributions read:

$$\mathcal{W}_u(\mathcal{P}) = \int_{\mathcal{P}} \vec{b} \cdot \vec{v} \, \mathrm{d}\Omega + \int_{\partial\mathcal{P}} \vec{t} \cdot \vec{v} \, \mathrm{d}\Gamma \,, \tag{11a}$$

$$\mathcal{Q}_u(\mathcal{P}) = \int_{\mathcal{P}} s_q \, \mathrm{d}\Omega - \int_{\partial\mathcal{P}} \vec{q} \cdot \vec{n} \, \mathrm{d}\Gamma \,, \tag{11b}$$

$$\mathcal{T}_u(\mathcal{P}) = \int_{\mathcal{P}} {}^u\mu_L \, s_L + {}^u\mu_T \, s_T \, \mathrm{d}\Omega - \int_{\partial\mathcal{P}} {}^u\mu_L \, \vec{h}_L \cdot \vec{n} \, \mathrm{d}\Gamma \,, \tag{11c}$$

where $\vec{t}$ is the surface traction, $\vec{v}$ is the velocity, s_q is the rate in energy per unit volume at which heat is generated by sources, and $\vec{q}$ is the flux of heat.

Since they are defined over a finite sub-part $\mathcal{P}$, the four quantities $\mathcal{U}$, $\mathcal{W}_u$, $\mathcal{Q}_u$, and $\mathcal{T}_u$ are scalar functions of time. The time variation of net internal energy $\mathcal{U}$ corresponds to the power expenditure of external agencies: a mechanical contribution $\mathcal{W}_u$ due to body forces $\vec{b}$ and surface tractions $\vec{t}$ that do work on velocities $\vec{v}$; a heat contribution $\mathcal{Q}_u$ where s_q is the heat supplied by external agencies and $\vec{q}$ is the heat flux vector; a mass contribution $\mathcal{T}_u$ in which the scalar ${}^u\mu_\beta$ denotes the change in specific energy provided by a unit supply of *moles* of species $\beta = L, T$. Such a scalar will be specified in section 3.6.

As usual in the thermodynamics of continua, see e.g. [23], one can make use of the specific internal energy u per unit volume

$$\mathcal{U}(\mathcal{P}) = \int_{\mathcal{P}} u \, \mathrm{d}\Omega \,.$$

In small displacements one can define specific internal energy per unit mass or per unit volume, since both mass and volume do not change during the process. We choose to define it per unit volume. Standard application of the divergence theorem and of balance equations (2, 3) leads from (11) to

$$\mathcal{W}_u(\mathcal{P}) = \int_{\mathcal{P}} \boldsymbol{\sigma} : \frac{\partial \boldsymbol{\varepsilon}}{\partial t} \, \mathrm{d}\Omega \,, \tag{12a}$$

$$\mathcal{Q}_u(\mathcal{P}) = \int_{\mathcal{P}} s_q - \mathrm{div}\,[\,\vec{q}\,] \, \mathrm{d}\Omega \,, \tag{12b}$$

$$\mathcal{T}_u(\mathcal{P}) = \int_{\mathcal{P}} {}^u\mu_L \, \frac{\partial c_L}{\partial t} + {}^u\mu_L \, w^{(1)} - \vec{h}_L \cdot \nabla\,[\,{}^u\mu_L\,] \, \mathrm{d}\Omega + \int_{\mathcal{P}} {}^u\mu_T \, \frac{\partial c_T}{\partial t} - {}^u\mu_T \, w^{(1)} \, \mathrm{d}\Omega \,. \tag{12c}$$

where ε is the strain tensor, i.e. $\frac{\partial \boldsymbol{\varepsilon}}{\partial t} = \mathrm{sym}\,[\,\nabla\,[\,\vec{v}\,]\,]$. The first law of thermodynamics is thus stated as follows:

$$\int_{\mathcal{P}} \frac{\mathrm{d}u}{\mathrm{d}t} \, \mathrm{d}\Omega = \int_{\mathcal{P}} \boldsymbol{\sigma} : \frac{\partial \boldsymbol{\varepsilon}}{\partial t} + s_q - \mathrm{div}\,[\,\vec{q}\,] + {}^u\mu_L \, \frac{\partial c_L}{\partial t} + {}^u\mu_T \, \frac{\partial c_T}{\partial t} - \vec{h}_L \cdot \nabla\,[\,{}^u\mu_L\,] + ({}^u\mu_L - {}^u\mu_T)\, w^{(1)} \, \mathrm{d}\Omega \,.$$

It must hold for any region $\mathcal{P}$, since the latter is arbitrary. The local form of the first principle thus reads:

$$\frac{\mathrm{d}u}{\mathrm{d}t} = \boldsymbol{\sigma} : \frac{\partial \boldsymbol{\varepsilon}}{\partial t} + s_q - \mathrm{div}\,[\,\vec{q}\,] + {}^u\mu_L \, \frac{\partial c_L}{\partial t} + {}^u\mu_T \, \frac{\partial c_T}{\partial t} - \vec{h}_L \cdot \nabla\,[\,{}^u\mu_L\,] + ({}^u\mu_L - {}^u\mu_T)\, w^{(1)} \,. \tag{13}$$

---

[3]Augmenting the energy balance with energy flows due to species transport is not always accomplished. Such a term is not included for instance in [21, 24] whereas it appears in [23] in a different fashion.

3.2 Entropy imbalance

The second law of thermodynamics represents the balance of the interplay among the internal entropy of $\mathcal{P}$ and the entropy transferred in $\mathcal{P}$ due to mass exchange and heat transferred on $\mathcal{P}$. The entropy balance for the problem at hand, for *quasi-static interactions*, reads:

$$\frac{\mathrm{d}\,\mathcal{S}}{\mathrm{d}t}(\mathcal{P}) - \frac{\mathrm{d}\,\mathcal{S}_i}{\mathrm{d}t}(\mathcal{P}) = \mathcal{Q}_\eta(\mathcal{P}) + \mathcal{T}_\eta(\mathcal{P}) \,, \tag{14}$$

where $\mathcal{S}$ is the net internal entropy of $\mathcal{P}$, $\mathcal{S}_i$ is the entropy produced inside $\mathcal{P}$, $\mathcal{Q}_\eta$ the entropy per unit time due to heat transfer, $\mathcal{T}_\eta$ the entropy per unit time due to mass transfer. The individual contributions read:

$$\mathcal{Q}_\eta(\mathcal{P}) = \int_\mathcal{P} \frac{s_q}{T} \, \mathrm{d}\Omega - \int_{\partial\mathcal{P}} \frac{\vec{q}}{T} \cdot \vec{n} \, \mathrm{d}\Gamma \,, \tag{15a}$$

$$\mathcal{T}_\eta(\mathcal{P}) = \int_\mathcal{P} {}^\eta\mu_L \, s_L + {}^\eta\mu_T \, s_T \, \mathrm{d}\Omega - \int_{\partial\mathcal{P}} {}^\eta\mu_L \, \vec{h}_L \cdot \vec{n} \, \mathrm{d}\Gamma \,. \tag{15b}$$

Equation (14) stems from the non-trivial assumption that mechanics does not contribute directly to the total entropy flow in the entropy balance equation. This assumption is profoundly elaborated in [21, 27]. The scalar ${}^\eta\mu_\beta$ denotes the change in specific entropy provided by a unit supply of *moles*[4] of species $\beta = L, T$. The second law of thermodynamics states that

$$\frac{\mathrm{d}\,\mathcal{S}_i}{\mathrm{d}t}(\mathcal{P}) \geq 0 \,.$$

One can make use of the specific internal entropy η per unit volume

$$\mathcal{S}(\mathcal{P}) = \int_\mathcal{P} \eta \, \mathrm{d}\Omega \,.$$

In small displacements one can define specific internal entropy per unit mass or per unit volume, since both mass and volume do not change during the process. We choose to define it per unit volume. Standard application of the divergence theorem and of mass balances (2) leads from (15) to

$$\frac{\mathrm{d}}{\mathrm{d}t} \int_\mathcal{P} \eta \, \mathrm{d}\Omega + \int_\mathcal{P} -\frac{s_q}{T} + \mathrm{div}\left[\frac{\vec{q}}{T}\right] - {}^\eta\mu_L \, s_L + \mathrm{div}\left[{}^\eta\mu_L \, \vec{h}_L\right] - {}^\eta\mu_T \, s_T \, \mathrm{d}\Omega \geq 0 \,. \tag{16}$$

By noting that

$$\mathrm{div}\left[\frac{\vec{q}}{T}\right] = \frac{1}{T} \mathrm{div}\left[\vec{q}\right] - \frac{1}{T^2} \vec{q} \cdot \nabla\left[T\right] \,,$$

taking advantage of identity (13) and of the sign definiteness of temperature, we can rephrase the entropy imbalance in terms of internal energy:

$$\int_\mathcal{P} T \frac{\mathrm{d}\eta}{\mathrm{d}t} - \frac{1}{T} \vec{q} \cdot \nabla\left[T\right] - T \, {}^\eta\mu_L \, s_L + T \, \mathrm{div}\left[{}^\eta\mu_L \, \vec{h}_L\right] - T \, {}^\eta\mu_T \, s_T \, \mathrm{d}\Omega +$$

$$-\left\{\int_\mathcal{P} \frac{\mathrm{d}u}{\mathrm{d}t} - \boldsymbol{\sigma} : \frac{\partial\boldsymbol{\varepsilon}}{\partial t} - {}^u\mu_L \frac{\partial c_L}{\partial t} - {}^u\mu_T \frac{\partial c_T}{\partial t} + \vec{h}_L \cdot \nabla\left[{}^u\mu_L\right] - \left({}^u\mu_L - {}^u\mu_T\right) w^{(1)} \, \mathrm{d}\Omega\right\} \geq 0 \,.$$

By exploiting mass balance equations (2), the entropy imbalance finally becomes

$$\int_\mathcal{P} T \frac{\mathrm{d}\eta}{\mathrm{d}t} - \frac{\mathrm{d}u}{\mathrm{d}t} \, \mathrm{d}\Omega +$$

$$+ \int_\mathcal{P} -\frac{1}{T} \vec{q} \cdot \nabla\left[T\right] - T \, {}^\eta\mu_L \frac{\partial c_L}{\partial t} - T \, {}^\eta\mu_T \frac{\partial c_T}{\partial t} + T \, \vec{h}_L \cdot \nabla\left[{}^\eta\mu_L\right] - T \, \left({}^\eta\mu_L - {}^\eta\mu_T\right) w^{(1)} \, \mathrm{d}\Omega +$$

$$- \int_\mathcal{P} -\boldsymbol{\sigma} : \frac{\partial\boldsymbol{\varepsilon}}{\partial t} - {}^u\mu_L \frac{\partial c_L}{\partial t} - {}^u\mu_T \frac{\partial c_T}{\partial t} + \vec{h}_L \cdot \nabla\left[{}^u\mu_L\right] - \left({}^u\mu_L - {}^u\mu_T\right) w^{(1)} \, \mathrm{d}\Omega \geq 0 \,.$$

---

[4]It is worth pointing out that [23] does not consider the contribution of mass to the flux of entropy in (14).

Denote with the symbol μ_β the quantity

$$\mu_\beta = {}^u\mu_\beta - T\,{}^\eta\mu_\beta \tag{17}$$

and with the symbol $A^{(1)}$ the following:

$$A^{(1)} = \mu_T - \mu_L \,, \tag{18}$$

in order to write the entropy imbalance as

$$\int_{\mathcal{P}} T\frac{\mathrm{d}\eta}{\mathrm{d}t} - \frac{\mathrm{d}u}{\mathrm{d}t} - \frac{1}{T}\vec{q}\cdot\nabla[T] + \mu_L\frac{\partial c_L}{\partial t} + \mu_T\frac{\partial c_T}{\partial t} +$$
$$-\vec{h}_L\cdot\nabla[\mu_L] - {}^\eta\mu_L\,\vec{h}_L\cdot\nabla[T] - w^{(1)}A^{(1)} + \boldsymbol{\sigma}:\frac{\partial\boldsymbol{\varepsilon}}{\partial t}\ \mathrm{d}\Omega \geq 0 \,.$$

Following [21] a new heat flux

$$\vec{\tilde{q}} = \vec{q} + T\,{}^\eta\mu_L\,\vec{h}_L \tag{19}$$

can be defined, whereby $T\,{}^\eta\mu_L\,\vec{h}_L$ represents the heat transfer due to diffusion of interstitial species in the lattice. $\vec{\tilde{q}}$ is the thermodynamic response conjugate to the gradient of temperature, i.e.:

$$\int_{\mathcal{P}} T\frac{\mathrm{d}\eta}{\mathrm{d}t} - \frac{\mathrm{d}u}{\mathrm{d}t} + \mu_L\frac{\partial c_L}{\partial t} + \mu_T\frac{\partial c_T}{\partial t} + \boldsymbol{\sigma}:\frac{\partial\boldsymbol{\varepsilon}}{\partial t}\ \mathrm{d}\Omega + \tag{20}$$
$$+ \int_{\mathcal{P}} -\frac{1}{T}\vec{\tilde{q}}\cdot\nabla[T] - \vec{h}_L\cdot\nabla[\mu_L] - w^{(1)}A^{(1)}\ \mathrm{d}\Omega \geq 0 \,.$$

3.3 Additive decompositions.

It is customary in non-equilibrium thermodynamics [24, 28] to additively decompose the stress into the sum of two symmetric tensors, an elastic part $\boldsymbol{\sigma}^e$ and a viscous, dissipative part $\boldsymbol{\sigma}^d$

$$\boldsymbol{\sigma} = \boldsymbol{\sigma}^e + \boldsymbol{\sigma}^d \,. \tag{21}$$

The elastic part is assumed to be derivable from a potential.

The strain tensor $\boldsymbol{\varepsilon}$ can be also additively decomposed into a chemo-thermo-elastic tensor $\boldsymbol{\varepsilon}^{cte}$ and into an inelastic contribution $\boldsymbol{\varepsilon}^{in}$, following a rather classical decomposition of strains in standard dissipative systems [29]:

$$\boldsymbol{\varepsilon} = \boldsymbol{\varepsilon}^{cte} + \boldsymbol{\varepsilon}^{in} \,. \tag{22}$$

The contribution $\boldsymbol{\sigma}:\frac{\partial\boldsymbol{\varepsilon}^{in}}{\partial t}$ has a dissipative nature, that will be discussed further in the paper. Tensor $\boldsymbol{\varepsilon}^{cte}$ will be subject to further additive decompositions, that will be introduced at a convenient time.

3.4 Helmholtz free energy.

Different thermodynamic potentials can be considered rather than the internal energy u. The specific *Helmholtz free energy* per unit volume ψ is defined as

$$\psi = u - T\,\eta \tag{23}$$

and will be used henceforth. It is taken as a function of temperature, concentrations, and the chemo-thermo-mechanical strain[5] and of some kinematic internal variables $\boldsymbol{\xi}$ that compare with the usual meaning

---

[5] This is not the only possible choice. Focusing on the functional dependence on the strain only, the Helmholtz free energy could be written as a function of the whole strain tensor and of its inelastic counterpart:

$$\psi = \psi(\boldsymbol{\varepsilon}, \boldsymbol{\varepsilon}^{in}, ...) \,.$$

In the Coleman-Noll procedure, the stress is finally related to the derivative of the Helmholtz free energy wrt to the total strain:

$$\boldsymbol{\sigma} = \frac{\partial\psi}{\partial\boldsymbol{\varepsilon}} \,.$$

In the realm of large strains, this approach has been taken for instance in [30, 31].

in inelastic constitutive laws. It follows that

$$T\frac{\mathrm{d}\eta}{\mathrm{d}t} - \frac{\mathrm{d}u}{\mathrm{d}t} = -\frac{\mathrm{d}\psi}{\mathrm{d}t} - \eta\frac{\partial T}{\partial t} , \tag{24}$$

which can be inserted in (20) to derive the entropy imbalance in final form:

$$\int_{\mathcal{P}} -\frac{\mathrm{d}\psi}{\mathrm{d}t} - \eta\frac{\partial T}{\partial t} + \mu_L\frac{\partial c_L}{\partial t} + \mu_T\frac{\partial c_T}{\partial t} + \boldsymbol{\sigma}^e : \frac{\partial \boldsymbol{\varepsilon}^{cte}}{\partial t} - \frac{1}{T}\vec{q}\cdot\nabla[T] + \tag{25}$$

$$-\vec{h}_L\cdot\nabla[\mu_L] - w^{(1)}A^{(1)} + \boldsymbol{\sigma}^d : \frac{\partial \boldsymbol{\varepsilon}^{cte}}{\partial t} + \boldsymbol{\sigma} : \frac{\partial \boldsymbol{\varepsilon}^{in}}{\partial t} \ \mathrm{d}\Omega \geq 0 .$$

In view of the stated functional dependency of the free energy, its total derivative with respect to time reads:

$$\frac{\mathrm{d}}{\mathrm{d}t}\psi(T,\boldsymbol{\varepsilon}^{cte},c_L,c_T,\boldsymbol{\xi}) = \frac{\partial\psi}{\partial T}\frac{\partial T}{\partial t} + \frac{\partial\psi}{\partial\boldsymbol{\varepsilon}^{cte}} : \frac{\partial\boldsymbol{\varepsilon}^{cte}}{\partial t} + \frac{\partial\psi}{\partial c_L}\frac{\partial c_L}{\partial t} + \frac{\partial\psi}{\partial c_T}\frac{\partial c_T}{\partial t} + \frac{\partial\psi}{\partial\boldsymbol{\xi}} : \frac{\partial\boldsymbol{\xi}}{\partial t} \tag{26}$$

The internal force, conjugate to $\boldsymbol{\xi}$, will be denoted with the symbol $\boldsymbol{\chi}$, i.e.

$$\boldsymbol{\chi} = -\frac{\partial\psi}{\partial\boldsymbol{\xi}} . \tag{27}$$

3.5 Thermodynamic restrictions.

Inequality (25) becomes:

$$\int_{\mathcal{P}} -\frac{\partial\psi}{\partial T}\frac{\partial T}{\partial t} - \frac{\partial\psi}{\partial\boldsymbol{\varepsilon}^{cte}} : \frac{\partial\boldsymbol{\varepsilon}^{cte}}{\partial t} - \frac{\partial\psi}{\partial c_L}\frac{\partial c_L}{\partial t} - \frac{\partial\psi}{\partial c_T}\frac{\partial c_T}{\partial t} - \frac{\partial\psi}{\partial\boldsymbol{\xi}} : \frac{\partial\boldsymbol{\xi}}{\partial t} +$$

$$-\eta\frac{\partial T}{\partial t} + \mu_L\frac{\partial c_L}{\partial t} + \mu_T\frac{\partial c_T}{\partial t} + \boldsymbol{\sigma}^e : \frac{\partial\boldsymbol{\varepsilon}^{cte}}{\partial t} - \frac{1}{T}\vec{q}\cdot\nabla[T] +$$

$$-\vec{h}_L\cdot\nabla[\mu_L] - w^{(1)}A^{(1)} + \boldsymbol{\sigma}^d : \frac{\partial\boldsymbol{\varepsilon}^{cte}}{\partial t} + \boldsymbol{\sigma} : \frac{\partial\boldsymbol{\varepsilon}^{in}}{\partial t} \ \mathrm{d}\Omega \geq 0$$

and must hold for any region $\mathcal{P}$, since the latter was arbitrarily taken. Therefore, the following *local* entropy imbalance, usually termed the Clausius-Duhem inequality, yields

$$\frac{\partial T}{\partial t}\left(-\eta - \frac{\partial\psi}{\partial T}\right) + \frac{\partial\boldsymbol{\varepsilon}^{cte}}{\partial t} : \left(\boldsymbol{\sigma}^e - \frac{\partial\psi}{\partial\boldsymbol{\varepsilon}^{cte}}\right) + \frac{\partial c_L}{\partial t}\left(\mu_L - \frac{\partial\psi}{\partial c_L}\right) + \frac{\partial c_T}{\partial t}\left(\mu_T - \frac{\partial\psi}{\partial c_T}\right) +$$

$$+\boldsymbol{\chi} : \frac{\partial\boldsymbol{\xi}}{\partial t} - \vec{h}_L\cdot\nabla[\mu_L] - w^{(1)}A^{(1)} - \frac{1}{T}\vec{q}\cdot\nabla[T] + \boldsymbol{\sigma}^d : \frac{\partial\boldsymbol{\varepsilon}^{cte}}{\partial t} + \boldsymbol{\sigma} : \frac{\partial\boldsymbol{\varepsilon}^{in}}{\partial t} \geq 0 . \tag{28}$$

This inequality must hold for any value of the time derivative of the temperature T, the concentrations c_L and c_T, the strain tensor $\boldsymbol{\varepsilon}^{cte}$. Since they appear linearly in the inequality, the factors multiplying them must be zero, as otherwise it would be possible to find a value for the time derivatives that violate the inequality. Therefore, the following restrictions apply

$$\boldsymbol{\sigma}^e = \left.\frac{\partial\psi}{\partial\boldsymbol{\varepsilon}^{cte}}\right|_{T,c_L,c_T,\boldsymbol{\xi}} , \qquad \eta = -\left.\frac{\partial\psi}{\partial T}\right|_{\boldsymbol{\varepsilon}^{cte},c_L,c_T,\boldsymbol{\xi}} ,$$

$$\mu_L = \left.\frac{\partial\psi}{\partial c_L}\right|_{T,\boldsymbol{\varepsilon}^{cte},c_T,\boldsymbol{\xi}} , \qquad \mu_T = \left.\frac{\partial\psi}{\partial c_T}\right|_{T,\boldsymbol{\varepsilon}^{cte},c_L,\boldsymbol{\xi}} . \tag{29}$$

In eq. (29) it has been explicitly pointed out which independent thermodynamic fields shall be taken as fixed in the definition of thermodynamic forces $\boldsymbol{\sigma}^e$, η, μ_L, μ_T. Equation (29) yields to the inequality:

$$\underbrace{\boldsymbol{\sigma}^d : \frac{\partial\boldsymbol{\varepsilon}^{cte}}{\partial t} + \boldsymbol{\sigma} : \frac{\partial\boldsymbol{\varepsilon}^{in}}{\partial t} + \boldsymbol{\chi} : \frac{\partial\boldsymbol{\xi}}{\partial t}}_{\text{inelastic}} - \underbrace{\vec{h}_L\cdot\nabla[\mu_L]}_{\text{diffusive}} - \underbrace{\frac{1}{T}\vec{q}\cdot\nabla[T]}_{\text{thermal}} - \underbrace{w^{(1)}A^{(1)}}_{\text{chemical}} \geq 0 \tag{30}$$

which is the internal entropy production (multiplied with the temperature). Mechanical, diffusive, chemical, and thermal contributions are devised as shown. Inequality (30) has the usual dissipative structure [32]. Under the assumptions of Curie symmetry principle [21], fluxes and thermodynamic forces of different tensorial character do not couple. Inequality (30) thus can be written as

$$\boldsymbol{\sigma}^d : \frac{\partial \boldsymbol{\varepsilon}^{cte}}{\partial t} + \boldsymbol{\sigma} : \frac{\partial \boldsymbol{\varepsilon}^{in}}{\partial t} + \boldsymbol{\chi} : \frac{\partial \boldsymbol{\xi}}{\partial t} \geq 0 \tag{31a}$$

$$-\vec{h}_L \cdot \nabla [\mu_L] - \frac{1}{T}\vec{q} \cdot \nabla [T] \geq 0 \tag{31b}$$

$$-w^{(1)} A^{(1)} \geq 0 \tag{31c}$$

Remark - In view of formula (29), the amount μ_β declared in eq. (17) acquires the meaning of *chemical potential* and hence the term $A^{(1)}$ turns out to be the *affinity of the reaction* (1).

Remark - The Helmholtz free energy density has been derived with respect to time in Eq.(26). Exploiting the thermodynamic restriction (29) for entropy and for stress, the result in Eq. (24) leads to

$$-T \frac{\mathrm{d}}{\mathrm{d}t}\frac{\partial \psi}{\partial T} = \frac{\mathrm{d}u}{\mathrm{d}t} - \boldsymbol{\sigma}^e : \frac{\partial \boldsymbol{\varepsilon}^{cte}}{\partial t} - \mu_L \frac{\partial c_L}{\partial t} - \mu_T \frac{\partial c_T}{\partial t} + \boldsymbol{\chi} : \frac{\partial \boldsymbol{\xi}}{\partial t} . \tag{32}$$

This identity will be used in Appendix B as the starting point to derive the generalized heat equation .

3.6 Specifications for $^u\mu_\beta$ and $^\eta\mu_\beta$.

Identity (29b) allows expression of the entropy as a function of temperature, concentrations, chemo-thermo-mechanical strain, and internal variables. Since the specific energy u is a function of entropy, it also becomes a function of the same thermodynamic variables set, i.e.

$$u = u(\eta(T, \boldsymbol{\varepsilon}^{cte}, c_L, c_T, \boldsymbol{\xi}), \boldsymbol{\varepsilon}^{cte}, c_L, c_T, \boldsymbol{\xi}) .$$

From the definition (23) of the Helmholtz free energy, it descends that

$$\frac{\partial}{\partial c_\beta}\psi(T, \boldsymbol{\varepsilon}^{cte}, c_L, c_T, \boldsymbol{\xi}) = \frac{\mathrm{d}u}{\mathrm{d}c_\beta} + T \frac{\partial}{\partial c_\beta}\frac{\partial \psi}{\partial T} , \tag{33}$$

with $\beta = L, T$. In view of (29), the term on the left hand side is the chemical potential of species β. We compute the entropy per mole $^\eta\mu_\beta$ as

$$^\eta\mu_\beta = \frac{\partial}{\partial c_\beta}\eta(T, \boldsymbol{\varepsilon}^{cte}, c_L, c_T, \boldsymbol{\xi}) = -\frac{\partial}{\partial c_\beta}\frac{\partial \psi}{\partial T} = -\frac{\partial}{\partial T}\frac{\partial \psi}{\partial c_\beta} = -\frac{\partial}{\partial T}\mu_\beta(T, \boldsymbol{\varepsilon}^{cte}, c_L, c_T, \boldsymbol{\xi}) . \tag{34}$$

It thus descends from declaration (17) that $^u\mu_\beta$ amounts to

$$^u\mu_L = \left. \frac{\mathrm{d}}{\mathrm{d}c_L}u(\eta(T, \boldsymbol{\varepsilon}^{cte}, c_L, c_T, \boldsymbol{\xi}), \boldsymbol{\varepsilon}^{cte}, c_L, c_T, \boldsymbol{\xi}) \right|_{T, c_T, \boldsymbol{\varepsilon}^{cte}, \boldsymbol{\xi}} , \tag{35a}$$

$$^u\mu_T = \left. \frac{\mathrm{d}}{\mathrm{d}c_T}u(\eta(T, \boldsymbol{\varepsilon}^{cte}, c_L, c_T, \boldsymbol{\xi}), \boldsymbol{\varepsilon}^{cte}, c_L, c_T, \boldsymbol{\xi}) \right|_{T, c_L, \boldsymbol{\varepsilon}^{cte}, \boldsymbol{\xi}} . \tag{35b}$$

Therefore, neither $^u\mu_\beta$ nor $^\eta\mu_\beta$ are partial molar quantities, since they are not defined at fixed temperature and stresses. This outcome is consistent with the local form of the first principle (13). It holds in fact:

$$\frac{\partial \psi}{\partial c_\beta} = \frac{\mathrm{d}u}{\mathrm{d}c_\beta} + T \frac{\partial}{\partial c_\beta}\frac{\partial \psi}{\partial T} = \frac{\partial u}{\partial c_\beta} + \frac{\partial u}{\partial \eta}\frac{\partial \eta}{\partial c_\beta} + T \frac{\partial}{\partial c_\beta}\frac{\partial \psi}{\partial T} = \frac{\partial u}{\partial c_\beta} = \mu_\beta \tag{36}$$

and

$$^u\mu_\beta = \frac{\mathrm{d}u}{\mathrm{d}c_\beta} = \frac{\partial u}{\partial c_\beta} + \frac{\partial u}{\partial \eta}\frac{\partial \eta}{\partial c_\beta} = \mu_\beta + T\,^\eta\mu_\beta , \tag{37}$$

in agreement with definition (17). In summary therefore,

$$
{}^{\eta}\mu_\beta \;\; = \;\; -\frac{\partial^2 \psi}{\partial c_\beta \partial T} \tag{38a}
$$

$$
{}^{u}\mu_\beta \;\; = \;\; \frac{\partial \psi}{\partial c_\beta} - T\,\frac{\partial^2 \psi}{\partial c_\beta \partial T} \;. \tag{38b}
$$

Remark - The identification (38) of the energetic and entropic contributions to the chemical potential provides a neat formulation for the entropy production inequality (31b). One writes in view of definition (19)

$$
-\vec{h}_L \cdot \nabla \left[\mu_L \right] - \frac{1}{T} \vec{q} \cdot \nabla \left[T \right] = -\vec{h}_L \cdot \left(\nabla \left[\mu_L \right] + {}^{\eta}\mu_L \nabla \left[T \right] \right) - \frac{1}{T} \vec{q} \cdot \nabla \left[T \right] \;.
$$

By means of Eq. (38), the vector $\nabla \left[\mu_L \right] + {}^{\eta}\mu_L \nabla \left[T \right]$ is independent upon the gradient of temperature, since it holds

$$
\nabla \left[\mu_L \right] + {}^{\eta}\mu_L \nabla \left[T \right] = \frac{\partial^2 \psi}{\partial c_L^2} \nabla \left[c_L \right] + \frac{\partial^2 \psi}{\partial c_L \partial c_T} \nabla \left[c_T \right] + \frac{\partial^2 \psi}{\partial c_L \partial \boldsymbol{\varepsilon}^{cte}} : \nabla \left[\boldsymbol{\varepsilon}^{cte} \right] + \frac{\partial^2 \psi}{\partial c_L \partial \boldsymbol{\xi}} : \nabla \left[\boldsymbol{\xi} \right] \;. \tag{39}
$$

4 Constitutive theory

There are several ways to satisfy the thermodynamic restriction (31b). A strategy that immediately descends from (31b) models the flux of interstitial species by Fickian-diffusion, and the "heat flux" $\vec{q}$ via Fourier's law, i.e.

$$
\vec{h}_L = -\boldsymbol{M}_L(c_L)\,\nabla \left[\mu_L \right] \;, \qquad \vec{q} = -\boldsymbol{K}\,\nabla \left[T \right] \;, \tag{40}
$$

by means of positive definite mobility and heat conductivity tensors $\boldsymbol{M}_L$ and $\boldsymbol{K}$, respectively. A cleaner and intuitive approach, which will be pursued from now on, relates the ordinary heat flux $\vec{q}$ to the gradient of temperature via Fourier's law, and relates the mass flux to the remaining gradients in view of Eq. (39) in a consistent way with the thermodynamic restriction (31b):

$$
\vec{h}_L \;\; = \;\; -\boldsymbol{M}_L(c_L)\,\left(\nabla \left[\mu_L \right] + {}^{\eta}\mu_L \nabla \left[T \right] \right) \tag{41a}
$$

$$
\vec{q} \;\; = \;\; -\boldsymbol{K}\,\nabla \left[T \right] \;. \tag{41b}
$$

More general approaches, which include the Soret effect of thermal diffusion and the Dufour effect of heat flow generated by concentration gradients, are obviously possible but will not be accounted for here.

The following isotropic non linear [33] specialization for the mobility tensor $\boldsymbol{M}_L$

$$
\boldsymbol{M}_L(c_L) = \natural_L\, c_L^{max}\, \theta_L\, (1 - \theta_L)\, \mathbb{1} \tag{42}
$$

accounts for saturation. In formula (42): $\theta_L = c_L/c_L^{max}$; c_L^{max} is the saturation limit for interstitial species. The *mobility* $\natural_L > 0$ represents the average velocity of interstitial species when acted upon by a force of 1 N/mol independent of the origin of the force. Definition (42) represents the physical requirement that both the pure ($c_L = 0$) and the saturated ($c_L = c_L^{max}$) phases have vanishing mobilities. Assuming that the trapped species have vanishing mobility is an alternative view of modeling the absence of trapped species flux. Neither the mobility $\natural_L$ nor the saturation concentration c_L^{max} are assumed to change in time. Such a limitation can be removed without altering the conceptual picture if experimental data indicate an influence of temperature, stresses, or concentrations.

The Helmholtz free energy density ψ is modeled by decomposing it into separate parts: a diffusive contribution ψ_{diff}, a thermal contribution ψ_{th}, an elastic contribution ψ_{el}, and an inelastic (or *defect energy* [23]) counterpart ψ_{in}

$$
\psi(c_L, c_T, T, \boldsymbol{\varepsilon}^{cte}, \boldsymbol{\xi}) = \psi_0 + \psi_{diff}(c_L, c_T, T, \boldsymbol{\xi}) + \psi_{th}(c_L, c_T, T) + \psi_{el}(\boldsymbol{\varepsilon}^{cte}, c_L, c_T, T) + \psi_{in}(c_L, c_T, T, \boldsymbol{\xi}) \;. \tag{43}
$$

This split is here taken for granted without motivation. A detailed analysis for the *microstructure term* ψ_{in} can be found in [34]. ψ_0 is a datum value.

The thermal contribution $\psi_{th}(c_L, c_T, T)$ is taken as

$$\psi_{th} = -c_H{}^\eta\mu_H^0(T-T_0) - \frac{1}{2}\frac{c_{vH}^0\,c_H}{T_0}(T-T_0)^2 - (c_L{}^\eta\mu_L^0 + c_T{}^\eta\mu_T^0)(T-T_0) - \frac{1}{2}\frac{c_{vL}^0 c_L + c_{vT}^0 c_T}{T_0}(T-T_0)^2 \ . \quad (44)$$

The subscript H designates the host material, which has concentration c_H in moles per unit volume. The specific heats c_{vH}^0, c_{vL}^0, and c_{vT}^0 are, by convention, energy per mole per degree Kelvin, and therefore we multiply it by concentration to convert the energy to energy per unit volume. Each species has its own specific heat, taken to be constant. We have included ${}^\eta\mu_H^0$, ${}^\eta\mu_L^0$, and ${}^\eta\mu_T^0$ to allow for entropy driven by thermal fluctuations[6].

Statistical mechanics provides a description of the entropy for isolated systems in terms of the density of states Ω, which in the case of two-state systems is the number of possible molecular configurations [25]. Making recourse to Stirling's approximation, one finds that the formula for combinations provides the following number of possible configurations of interstitial species atoms in an ideal crystalline lattice

$$\Omega_L = \left[\theta_L^{\theta_L}\,(1-\theta_L)^{(1-\theta_L)}\right]^{-N_A\,c_L^{max}} \ , \quad (45)$$

having denoted Avogadro's number with N_A. Inserting (45) into Boltzmann's equation

$$\eta_L^{diff} = k_B\,\ln\Omega_L \ , \quad (46)$$

one finds that the following well-known expression of the entropy arises, since the universal gas constant R is the product of Boltzmann constant k_B and Avogadro's number:

$$\eta_L^{diff} = -R\,c_L^{max}\,(\theta_L\,\ln[\theta_L] + (1-\theta_L)\,\ln[1-\theta_L]) \ . \quad (47)$$

The η_T counterpart can be derived from the entropy Ω_T of the trapped species in terms of $\theta_T = c_T/c_T^{max}$ where the saturation limit for trapped species $c_T^{max}(\boldsymbol{\xi})$ may change in time due to inelastic deformations, accounted for by means of $\boldsymbol{\xi}$:

$$\eta_T^{diff} = -R\,c_T^{max}(\boldsymbol{\xi})\,(\theta_T(\boldsymbol{\xi})\,\ln[\theta_T(\boldsymbol{\xi})] + (1-\theta_T(\boldsymbol{\xi}))\,\ln[1-\theta_T(\boldsymbol{\xi})]) \ . \quad (48)$$

The free energy density (per unit volume) of mobile guest atoms interacting with a host medium is described by a regular solution model [33, 22], which provides the following free energy density for the continuum approximation of mixing:

$$\psi_{diff}(c_L, c_T, T, \boldsymbol{\xi}) = \mu_L^0\,c_L \ - \ T\eta_L^{diff} + \mu_T^0\,c_T \ - \ T\eta_T^{diff} + \ RT\,c_L^{max}\,\chi\,\theta_L\,(1-\theta_L) \ . \quad (49)$$

The model of the Helmholtz free energy density in Eq. (49) represents the entropy of mixing plus energetic interactions. The terms μ_L^0 and μ_T^0 are reference values of chemical potentials that specify the free energy in the absence of interaction and entropic contributions, and specify the trap binding energy ΔE_τ (i.e. the negative of the Gibbs free energy change), and in turn are related to the *equilibrium constant* K_{eq} of reaction (1) :

$$\Delta E_\tau = \mu_L^0 \ - \ \mu_T^0 \ = RT\,\ln[K_{eq}] \ . \quad (50)$$

The real valued constant χ in Eq. (49) - termed the *exchange parameter* [25] - characterizes the energy of interaction between mobile guest species and insertion sites. If all of the interactions between mobile species and sites are the same, then $\chi = 0$ and there is no energy of mixing: mixing is the ideal and purely entropic. The contribution $RT\,c_L^{max}\,\chi\,\theta_L\,(1-\theta_L)$, known as the excess Gibbs energy, endows the free energy density

---

[6]Note that perfect gas theory suggests that there should also be a term containing the logarithm of density to fully characterize the entropy due to thermal fluctuations, but we omit this term as having negligible increments, and therefore its effect is lumped into ψ_0

with a non convex behavior with respect to c_L for $\chi > 2$, which in turn may lead to phase segregation [35, 36, 37].

The chemo-thermo-elastic strain $\boldsymbol{\varepsilon}^{cte}$ is considered to be made up of three separate contributions: an elastic recoverable part after unloading $\boldsymbol{\varepsilon}^{el}$, a swelling contribution due to the insertion of species in the host material $\boldsymbol{\varepsilon}^s$, and a thermal distortion $\boldsymbol{\varepsilon}^{th}$:

$$\boldsymbol{\varepsilon}^{cte} = \boldsymbol{\varepsilon}^{el} + \boldsymbol{\varepsilon}^s + \boldsymbol{\varepsilon}^{th} . \tag{51}$$

The swelling contribution

$$\boldsymbol{\varepsilon}^s = \omega_L \left(c_L - c_L^0 \right) \mathbb{1} + \omega_T \left(c_T - c_T^0 \right) \mathbb{1} \tag{52}$$

is assumed to be volumetric and proportional to the deviation $c_\beta - c_\beta^0$ from the reference concentration c_β^0 by means of the chemical expansion coefficients ω_β of species β. They equal one third of the partial molar volumes at a given temperature. Symbol $\mathbb{1}$ denotes the identity matrix. The thermal strain tensor, purely volumetric as for the swelling contribution, is assumed to be proportional to the difference with respect to a reference temperature T_0, by means of the factor α termed the thermal expansion coefficient:

$$\boldsymbol{\varepsilon}^{th} = \alpha \left(T - T_0 \right) \mathbb{1} . \tag{53}$$

A possible choice for the elastic part of the free energy density $\psi_{el}(\boldsymbol{\varepsilon}^{cte}, c_L, c_T, T)$ in the small strain range is the usual quadratic form

$$\psi_{el}(\boldsymbol{\varepsilon}^{cte}, c_L, c_T, T) = \frac{1}{2} K(c_L, c_T, T) \operatorname{tr} \left[\boldsymbol{\varepsilon}^{cte} - \boldsymbol{\varepsilon}^s - \boldsymbol{\varepsilon}^{th} \right]^2 + G(c_L, c_T, T) \, || \operatorname{dev} \left[\boldsymbol{\varepsilon}^{cte} - \boldsymbol{\varepsilon}^s - \boldsymbol{\varepsilon}^{th} \right] ||^2 , \tag{54}$$

where K, G are the bulk and shear modulus respectively and they are made dependent on temperature and species concentrations. The stress tensor $\boldsymbol{\sigma}^e(\boldsymbol{\varepsilon}^{cte}, c_L, c_T, T)$ descends from the thermodynamic restriction (29a)

$$\boldsymbol{\sigma}^e = 2 \, G \operatorname{dev} \left[\boldsymbol{\varepsilon}^{cte} \right] + K \left\{ \operatorname{tr} \left[\boldsymbol{\varepsilon}^{cte} \right] - 3 \left[\omega_L \left(c_L - c_L^0 \right) + \omega_T \left(c_T - c_T^0 \right) + \alpha \left(T - T_0 \right) \right] \right\} \mathbb{1} . \tag{55}$$

Note that the derivative $\partial \psi_{el} / \partial c_\beta$, with $\beta = L, T$, is the sum of two contributions

$$\frac{\partial \psi_{el}}{\partial c_\beta} = -\omega_\beta \operatorname{tr} \left[\boldsymbol{\sigma}^e \right] + \frac{1}{2} \frac{\partial K}{\partial c_\beta} \operatorname{tr} \left[\boldsymbol{\varepsilon}^{cte} - \boldsymbol{\varepsilon}^s - \boldsymbol{\varepsilon}^{th} \right]^2 + \frac{\partial G}{\partial c_\beta} \, || \operatorname{dev} \left[\boldsymbol{\varepsilon}^{cte} - \boldsymbol{\varepsilon}^s - \boldsymbol{\varepsilon}^{th} \right] ||^2 . \tag{56}$$

The first emanates from the swelling part of the strain, and is present even if the material properties are independent on concentration of species. Analogously,

$$\frac{\partial \psi_{el}}{\partial T} = -\alpha \operatorname{tr} \left[\boldsymbol{\sigma}^e \right] + \frac{1}{2} \frac{\partial K}{\partial T} \operatorname{tr} \left[\boldsymbol{\varepsilon}^{cte} - \boldsymbol{\varepsilon}^s - \boldsymbol{\varepsilon}^{th} \right]^2 + \frac{\partial G}{\partial T} \, || \operatorname{dev} \left[\boldsymbol{\varepsilon}^{cte} - \boldsymbol{\varepsilon}^s - \boldsymbol{\varepsilon}^{th} \right] ||^2 . \tag{57}$$

Inelastic internal entropy production (30) was described by the internal flux variables $\boldsymbol{\varepsilon}^{in}, \boldsymbol{\xi}$ and by their energy-conjugate forces $\boldsymbol{\sigma}, \boldsymbol{\chi}$. The existence of a convex dissipation potential is often assumed as a function of the flux variables, being non-negative and zero at the origin. Internal forces that drive the irreversible processes are linked to the flux variables via normality rules after enforcement of the principle of maximum dissipation [38, 39]. Complementarity laws are more often expressed after a Legendre transformation, in the form of evolution laws of flux variables as a function of the internal forces:

$$\frac{\partial \boldsymbol{\varepsilon}^{in}}{\partial t} = \frac{\partial \varphi^{in}}{\partial \boldsymbol{\sigma}} , \qquad \frac{\partial \boldsymbol{\xi}}{\partial t} = \frac{\partial \varphi^{in}}{\partial \boldsymbol{\chi}} . \tag{58}$$

Standard J_2 flow theory with isotropic hardening and visco-plasticity of Perzyna type are considered in the numerical examples in section 7.

From Eq. (29) we derive the chemical potential of species $\beta = L, T$ as

$$\mu_\beta = \mu_\beta^0 - {}^\eta\mu_\beta^0 \left(T - T_0 \right) - \frac{1}{2} \frac{c_{v\beta}^0}{T_0} (T - T_0)^2 + RT \ln[\frac{\theta_\beta}{1 - \theta_\beta}] + RT \chi (1 - 2\theta_\beta) + \frac{\partial \psi_{el}}{\partial c_\beta} + \frac{\partial \psi_{in}}{\partial c_\beta} . \tag{59}$$

From Eq. (38a), the entropic contribution of the chemical potential reads:

$$^{\eta}\mu_\beta = -^{\eta}\mu_\beta^0 - \frac{c_{v\beta}^0}{T_0}(T - T_0) + R\,\ln[\frac{\theta_\beta}{1-\theta_\beta}] + R\,\chi(1-2\theta_\beta) + \frac{\partial^2\psi_{el}}{\partial T\partial c_\beta} + \frac{\partial^2\psi_{in}}{\partial T\partial c_\beta} \ . \tag{60}$$

By defining as usual the *interstitial diffusivity* by $\mathbb{D}_L = \mathbb{\mu}_L\,R\,T$, Fick's law (41a) becomes:

$$\vec{h}_L(c_L, c_T, T, \boldsymbol{\varepsilon}^{cte}, \boldsymbol{\xi}) = -\,\mathbb{D}_L\,[1 - 2\chi\,\theta_L\,(1-\theta_L)]\,\nabla[c_L] +$$

$$-\,\boldsymbol{M}(c_L)\,\left[\frac{\partial^2\psi_{el}}{\partial c_L^2}\,\nabla[c_L] + \frac{\partial^2\psi_{el}}{\partial c_L\partial c_T}\,\nabla[c_T] + \frac{\partial^2\psi_{el}}{\partial c_L\partial\boldsymbol{\varepsilon}^{cte}}\,:\,\nabla[\boldsymbol{\varepsilon}^{cte}]\right] +$$

$$-\,\boldsymbol{M}(c_L)\,\left[\frac{\partial^2\psi_{in}}{\partial c_L^2}\,\nabla[c_L] + \frac{\partial^2\psi_{in}}{\partial c_L\partial c_T}\,\nabla[c_T] + \frac{\partial^2\psi_{in}}{\partial c_L\partial\boldsymbol{\varepsilon}^{cte}}\,:\,\nabla[\boldsymbol{\varepsilon}^{cte}] + \frac{\partial^2\psi_{in}}{\partial c_L\partial\boldsymbol{\xi}}\,:\,\nabla[\boldsymbol{\xi}]\right] \ . \tag{61}$$

By comparing (61) with the mass flux formula for infinitely diluted solutions, that can be easily derived by taking $c_L^{max} \to \infty$, one concludes that saturation has no effect on the diffusivity $\mathbb{D}_L$: in fact, the impact of saturation on the mobility tensor and on the chemical potential act one against the other and the effects cancel out in the evaluation of diffusivity. Saturation does affect mass transport by mechanical and thermal effects, even under the simple assumption that material parameters are not influenced by the interstitial concentration of species. In the simple case of $\psi_{in} = 0$ with constant K and G, the mass flux becomes

$$\vec{h}_L = -\,\mathbb{D}_L\,[1 - 2\chi\,\theta_L\,(1-\theta_L)]\,\nabla[c_L] - 3\,\boldsymbol{M}(c_L)\,K\omega_L\,\left[3\,\omega_L\,\nabla[c_L] + 3\,\omega_T\,\nabla[c_T] - \nabla\left[\mathrm{tr}\left[\boldsymbol{\varepsilon}^{cte}\right]\right]\right] \ .$$

5 Chemical kinetics

For ideal systems, in which the solvent (if any) does not take part in reactions and the chemical potentials have entropy and energy contributions only, the chemical kinetics of reaction (1) is often modeled via the law of mass action [21]:

$$w^{(1)} = k_T\,\frac{\theta_L}{1-\theta_L} - k_L\,\frac{\theta_T}{1-\theta_T} \ , \tag{62a}$$

where k_T is the positive rate constant for the forward reaction (yielding trapped products T) and k_L the rate constant for the reverse reaction. Elastic and swelling contributions suggest some modifications to this form of the law of mass action. It is proposed here that factors k_L and k_T are no longer constant, but depend on the stress and on the concentrations (via elastic parameters) in the following way:

$$k_L = \tilde{k}_L\,\exp\frac{\partial\psi_{el}/\partial c_T}{R\,T}\,\exp\frac{\partial\psi_{in}/\partial c_T}{R\,T}\,\exp\frac{-^{\eta}\mu_T^0(T - T_0)}{R\,T}\,\exp\frac{-c_{vT}^0(T - T_0)^2}{2R\,T\,T_0} \tag{62b}$$

$$k_T = \tilde{k}_T\,\exp\frac{\partial\psi_{el}/\partial c_L}{R\,T}\,\exp\frac{\partial\psi_{in}/\partial c_L}{R\,T}\,\exp\frac{-^{\eta}\mu_L^0(T - T_0)}{R\,T}\,\exp\frac{-c_{vL}^0(T - T_0)^2}{2R\,T\,T_0}\,\exp\left[\chi(1-2\theta_L)\right] \ . \tag{62c}$$

with $\tilde{k}_T$ and $\tilde{k}_L$ constants and derivatives as in Eq. (56). This new formulation is consistent with the usual mass action law, which is recovered when elastic, swelling, and interaction contributions vanish.

The condition of null affinity $A^{(1)} = 0$ can be resolved for the Gibbs free energy change $\mu_L^0 - \mu_T^0$. From definition (18), formulae (50) and (93) the *equilibrium constant of reaction* (1) can be derived with simple algebra *at equilibrium conditions*:

$$K_{eq} = \frac{\theta_T^{eq}}{1-\theta_T^{eq}}\,\frac{1-\theta_L^{eq}}{\theta_L^{eq}}\,\exp\frac{\left[\frac{\partial\psi_{el}}{\partial c_T} - \frac{\partial\psi_{el}}{\partial c_L}\right]^{eq}}{R\,T}\,\exp\frac{\left[\frac{\partial\psi_{in}}{\partial c_T} - \frac{\partial\psi_{in}}{\partial c_L}\right]^{eq}}{R\,T}\,\exp\left[-\chi(1-2\theta_L^{eq})\right]\,\times \tag{63}$$

$$\times\,\exp\frac{(^{\eta}\mu_L^0 - ^{\eta}\mu_T^0)(T - T_0)}{R\,T}\,\exp\frac{(c_{vL}^0 - c_{vT}^0)(T - T_0)^2}{2R\,T\,T_0} \ .$$

Equilibrium concentrations of trapped and mobile species depend on temperature T and on the state of stress. The rates of the forward and backward reactions are equal at equilibrium, and the equilibrium constant, in the alternative form $K_{eq} = \tilde{k}_T/\tilde{k}_L$, can be derived from the mass action law (62a) by imposing $w^{(1)} = 0$. Identity (63) is recovered, consistently. Such an identity agrees well and extends *van't Hoff* relation that is often [25] used to model the temperature and pressure dependence of K_{eq}.

The thermodynamic restriction

$$w^{(1)} A^{(1)} \leq 0$$

is satisfied using Eq.(62). To prove this statement, define with

$$
\aleph = \exp \frac{\frac{\partial \psi_{el}}{\partial c_L} - \frac{\partial \psi_{el}}{\partial c_T}}{RT} \; \exp \frac{\frac{\partial \psi_{in}}{\partial c_L} - \frac{\partial \psi_{in}}{\partial c_T}}{RT} \; \exp \frac{({}^\eta \mu_T^0 - {}^\eta \mu_L^0)(T - T_0)}{RT} \; \times
$$
$$
\times \exp \frac{(c_{vT}^0 - c_{vL}^0)(T - T_0)^2}{2RTT_0} \; \exp \left[\chi \left(1 - 2\theta_L \right) \right] \; .
$$

The affinity and the reaction rate can be written as:

$$
A^{(1)} = RT \ln \left[\frac{\theta_T}{1 - \theta_T} \frac{1 - \theta_L}{\theta_L} \frac{1}{\aleph} \frac{1}{K_{eq}} \right] \; ,
$$
$$
w^{(1)} = \tilde{k}_L \left\{ -\frac{\theta_T}{1 - \theta_T} + \frac{\theta_L}{1 - \theta_L} \aleph K_{eq} \right\} \; .
$$

If $w^{(1)} > 0$ then

$$
\aleph > \frac{\theta_T}{1 - \theta_T} \frac{1 - \theta_L}{\theta_L} \frac{1}{K_{eq}}
$$

and in turn $A^{(1)} < 0$. Viceversa if $w^{(1)} < 0$ then $A^{(1)} > 0$.

A classical way to enforce thermodynamic restrictions for the reaction (1) is to linearly relate the affinity and the reaction rate, by means of a phenomenological coefficient $L^{(1)} > 0$:

$$w^{(1)} = -L^{(1)} A^{(1)} \tag{64}$$

It was remarked in [21] that the linear phenomenological Eq.(64) is not *a priory* satisfactory for chemical reactions, although there is always a region close to equilibrium where it holds. From the equations (93) for the chemical potentials, the law of mass action in fact leads to:

$$
w^{(1)} = \tilde{k}_T \; \exp \left[\frac{\mu_L - \mu_L^0}{RT} \right] - \tilde{k}_L \; \exp \left[\frac{\mu_T - \mu_T^0}{RT} \right] \; .
$$

With simple mathematical manipulations one derives

$$
w^{(1)} = \tilde{k}_L \; \exp \left[\frac{\mu_T - \mu_T^0}{RT} \right] \left(\exp \left[-\frac{A^{(1)}}{RT} \right] - 1 \right) \; , \tag{65}
$$

where $\mu_T - \mu_T^0$ can be expressed from Eq. (93) as a function of c_L, c_T, ε, T. Eq. (65) can be linearized for $A^{(1)}$ around the equilibrium configuration, in which the latter vanishes:

$$
w^{(1)} = -\tilde{k}_L \; \exp \left[\left. \frac{\mu_T - \mu_T^0}{RT} \right|^{eq} \right] \frac{A^{(1)}}{RT} + o(A^{(1)}) \; . \tag{66}
$$

By direct comparison of (64) and (66), coefficient $L^{(1)}$ reads:

$$
L^{(1)} = \tilde{k}_L \; \exp \left[\left. \frac{\mu_T - \mu_T^0}{RT} \right|^{eq} \right] = \tilde{k}_T \; \exp \left[\left. \frac{\mu_L - \mu_L^0}{RT} \right|^{eq} \right]
$$

and is always positive.

Species trapping was also pursued by Thomas and Chopin [40], who evaluated the rate of species exchange following the approach of McNabb and Foster [1]. The latter was used in place of the law of mass action. Such an approach falls beyond the scope of the present contribution.

5.1 Infinitely fast kinetics

In many circumstances, the rate limiting process in a multi-physics problem is, by far, often something other than the chemical reaction. For instance: i) the trapping and untrapping of hydrogen in dislocation cores is much faster than its diffusion in the host metal lattice [2, 7]; ii) the kinetics of transformation of high-affinity to low affinity integrins and vice versa in focal adhesions is much faster than the diffusion of the low-affinity integrin itself across the lipid bilayer membrane [17]. In such events it can be assumed that the reaction kinetics is infinitely fast, in the sense that the time required to reach chemical equilibrium is orders of magnitude smaller than the time-scale of other processes. The concentrations of trapped and interstitial species is then governed by thermodynamic equilibrium at all times, and the trapped concentration c_T can be related to the interstitial one by the equation $A^{(1)} = 0$, i.e.

$$\mu_T = \mu_L \qquad \forall\, c_L, \boldsymbol{\varepsilon}, T , \tag{67}$$

with chemical potentials from Eq. (93).

6 Governing equations

Governing equations can be derived by incorporating the constitutive equations (41b), (55), (61), and the mass action law (62) into the balance equations (2), (3), and (32). Specifically, by using Eqs. (13), (38), (43), (44), (49), (54), and (62) the energy balance (32) can be written as in the Eq.(68d) below. The lengthy algebra that leads to the generalized heat equation is collected in Appendix B.

Governing equations are written in term of concentrations c_L and c_T, displacements $\vec{u}$, and temperature T as:

using (61) and (62)

$$\frac{\partial c_L}{\partial t} + \mathrm{div}\left[\, \vec{h}_L(c_L, c_T, T, \boldsymbol{\varepsilon}^{cte}, \boldsymbol{\xi}\,)\right] + w^{(1)}(c_L, c_T, T, \boldsymbol{\varepsilon}^{cte}, \boldsymbol{\xi}\,) = s_L , \tag{68a}$$

using (62)

$$\frac{\partial c_T}{\partial t} - w^{(1)}(c_L, c_T, T, \boldsymbol{\varepsilon}^{cte}, \boldsymbol{\xi}\,) = s_T , \tag{68b}$$

using (55)

$$\mathrm{div}\left[\, \boldsymbol{\sigma}(\boldsymbol{\varepsilon}^{cte}, c_L, c_T, T)\right] + \vec{b} = \vec{0} , \tag{68c}$$

using (13), (38), (43), (44), (49), (54), and (62)

$$-T\frac{\partial^2 \psi}{\partial T^2}\frac{\partial T}{\partial t} - \mathrm{div}\left[\, \boldsymbol{K}\, \nabla\left[T\right]\right] = s_q + T\frac{\partial^2 \psi}{\partial T \partial \boldsymbol{\varepsilon}^{cte}} : \frac{\partial \boldsymbol{\varepsilon}^{cte}}{\partial t} + T\frac{\partial^2 \psi}{\partial T \partial \boldsymbol{\xi}} : \frac{\partial \boldsymbol{\xi}}{\partial t} + \boldsymbol{\sigma}^d : \frac{\partial \boldsymbol{\varepsilon}^{cte}}{\partial t} +$$

$$+\, \boldsymbol{\sigma} : \frac{\partial \boldsymbol{\varepsilon}^{in}}{\partial t} - \vec{h}_L \cdot \nabla\left[\,{}^u\mu_L\right] + \left({}^u\mu_L - {}^u\mu_T\right) w^{(1)} . \tag{68d}$$

Equations (68) are accompanied by non linear evolution equations for the viscous stress $\boldsymbol{\sigma}^d$, the inelastic strain tensor $\boldsymbol{\varepsilon}^{in}$, and for $\boldsymbol{\xi}$. Boundary conditions

$$\vec{h}_L \cdot \vec{n} = \overline{h} \qquad \vec{x} \in \partial^N V , \tag{69a}$$

$$\vec{q} \cdot \vec{n} = \overline{q} \qquad \vec{x} \in \partial^N V , \tag{69b}$$

$$\boldsymbol{\sigma} \cdot \vec{n} = \vec{\overline{p}} \qquad \vec{x} \in \partial^N V , \tag{69c}$$

are imposed along Neumann boundaries $\partial^N V$. To ensure solvability of the problem, Dirichlet boundary conditions have to be enforced along $\partial^D V$, where $\partial V = \partial^D V \cup \partial^N V$ and $\partial^D V \cap \partial^N V = \emptyset$.

$$T = \overline{T} \qquad \vec{x} \in \partial^D V , \tag{70}$$

$$u = \overline{u} \qquad \vec{x} \in \partial^D V . \tag{71}$$

As assessed in [41], Dirichlet boundary conditions for concentration should not be imposed. The correct boundary condition that enforces equilibrium will be written as an equivalence of chemical potentials. An example will be discussed in section 7.

Initial conditions are usually imposed for the concentration of interstitial species $c_L(\vec{x}, t = 0)$ as well as of trapped species $c_T(\vec{x}, t = 0)$ and temperature $T(\vec{x}, t = 0)$. To comply with equilibrium thermodynamics these conditions are uniform in volume V and equal to concentrations that are in equilibrium with external species. Balance of momentum, together with boundary conditions, provide the necessary and sufficient equations to solve for $\vec{u}$ at $t = 0$.

It is usual in plasticity to make use of the so-called *three-fields formulation*, in which the pressure is treated as an independent variable not characterized constitutively, whereas Eq.(29a) only applies in its deviatoric projection. Such a formulation develops from the Hu-Washizu functional, and the weak formulation of the problem derives from its stationarity with respect to its three fields [42]. It is advantageous to build a *three-field like* weak form for the governing equations (68), because the higher order derivatives involving the trace of the stress tensor can be dealt with numerically in a more effective way. This approach has been taken in building the weak form of the governing equations, prior to the numerical approximation via finite elements.

7 Case-studies

Three case studies are here dealt with. The first concerns the diffusion of vacancies in an aluminum lattice, induced by a stress field. The diffusion of vacancies is an isothermal process, which occurs without trapping and is thus a simple benchmark for the model described in the previous sections, which has been implemented within a user element (UEL) subroutine of Abaqus/Standard 2013. The outcomes have been compared with Villani et al. [43].

The general framework of thermo-chemo-mechanics with trapping applies well to the phenomena of hydrogen embrittlement in metals, which is considered as a second case-study. The transport model developed by Krom and co-workers [6, 7], which emanates from the work of Sofronis and McMeeking [5], fits perfectly the thermodynamic setting discussed in this paper. Both models investigate the effect of hydrostatic stress and trapping on the hydrogen distribution in a plastically deforming specimen steel, assuming that hydrogen atoms diffuse through the lattice, that trap sites are filled by lattice diffusion, and that additional traps are generated by plastic deformation.

The insertion, diffusion, and trapping of ionic lithium in active particles within battery cells is studied as the last example. These events alter the chemo-thermo-mechanical properties of the lithiated phase and cause a significant swelling of the hosting particle, thus generating a stress field and influencing the alloying reaction kinetics. Specific dimensionless quantities govern the evolution process, controlled either by transport or by chemical reactions. The implications in terms of phase segregation and capability of delithiation, i.e. capacity fade after the first lithiation, are investigated.

7.1 Redistribution of vacancies in metals

The redistribution of vacancies in a crystal lattice induced by the stress due to a far-field load is studied on an ideally infinite aluminum plate with a central circular hole of radius $\overline{R} = 1$ μm, see Fig. 1.

The number of vacancies in moles per unit volume is denoted with c_L. Since the diffusion of vacancies occurs without trapping, neither c_T nor $w^{(1)}$ are defined. Furthermore, since the process takes place under thermal equilibrium conditions, there is no evolution of temperature. Finally, to compare with Villani et al. [43], energetic interactions have been discarded (i.e. $\chi = 0$). Material properties, K and G, have been taken as independent of vacancy concentration[7]. Following the assumption of elastic perfectly plastic (EPP) material response adopted by [43], no hardening is accounted for. Neither internally generated vacancies, $s_L = 0$, nor body forces have been considered, $\vec{b} = \vec{0}$.

---

[7]To be compared against equations (12) and (33) in [43]. The chemical expansion coefficient ω_L replaces coefficient $\frac{\Delta v}{3}$ used in the reference, where Δv was defined as the relaxed lattice volume after one mole of atoms is removed from the lattice.
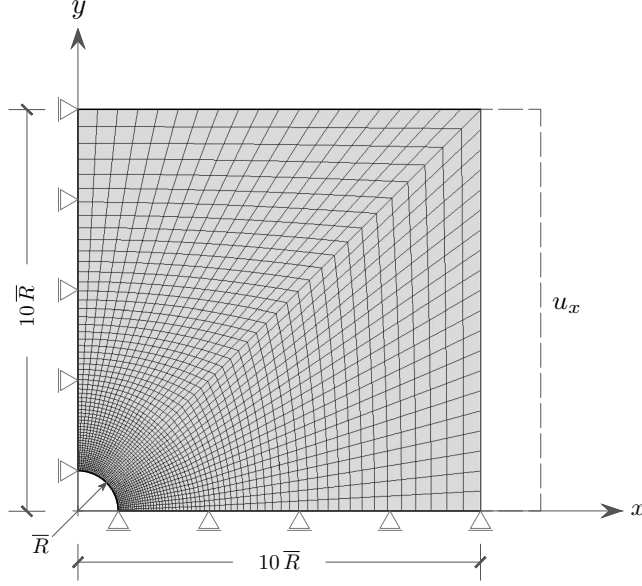
Figure 1: *Geometry and mechanical boundary conditions: $\overline{R}$ is the radius of the hole and $10\,\overline{R}$ the length of the edges. A tessellation of 2400 elements is displayed, too.*

The set of governing equations (68) rewrites as follows

$$\frac{\partial c_L}{\partial t} + \operatorname{div}\left[\,\vec{h}_L\,(\,c_L,\boldsymbol{\varepsilon}^{cte}\,)\,\right] = 0 \tag{72a}$$

$$\operatorname{div}\left[\,\boldsymbol{\sigma}\,(\,c_L,\boldsymbol{\varepsilon}^{cte}\,)\,\right] = \vec{0}\,, \tag{72b}$$

where the definition of the mass flux (61) under the assumption of infinitely diluted solution reduces to

$$\vec{h}_L\,(\,c_L,\boldsymbol{\varepsilon}^{cte}\,) = -\mathbb{D}_L\,\nabla\,[\,c_L\,] - 3\,\frac{K\,\omega_L\,\mathbb{D}_L}{R\,T}\,c_L\,\left[\,3\,\omega_L\,\nabla\,[\,c_L\,] - \nabla\,\left[\,\operatorname{tr}\left[\,\boldsymbol{\varepsilon}^{cte}\,\right]\,\right]\,\right]\,. \tag{73}$$

Cauchy's stress $\boldsymbol{\sigma}$ identifies with $\boldsymbol{\sigma}^e$ in equation (55) and reads:

$$\boldsymbol{\sigma}\,(\,c_L,\boldsymbol{\varepsilon}^{cte}\,) = 2\,G\,\operatorname{dev}\left[\,\boldsymbol{\varepsilon}^{cte}\,\right] + K\,\left[\,\operatorname{tr}\left[\,\boldsymbol{\varepsilon}^{cte}\,\right] - 3\,\omega_L\,\left(\,c_L - c_L^0\,\right)\,\right]\,\mathbb{1}\,. \tag{74}$$

The definitions of the yield stress σ_Y and of von Mises yield criterion for an elastic perfectly plastic material

$$\varphi^{in}(\boldsymbol{\sigma}) = ||\operatorname{dev}\left[\,\boldsymbol{\sigma}\,\right]|| - \sqrt{\frac{2}{3}}\,\sigma_Y = 0 \tag{75}$$

complete the formulation, together with the evolution law (58).

The resulting weak form (9) can be transformed in a first order ordinary differential equation in time if discretization is performed via space-time separated variables, with spatial dependent test and shape functions, whereas nodal unknowns depend solely on time. A family of time-advancing methods based on the so-called θ-scheme can be set up assuming that solution $y(t)$ is given at time t, and that the algorithm is triggered by the initial conditions at time $t = 0$. The backward Euler scheme ($\theta = 1$) has been selected. A Newton-Raphson iterative algorithm has been implemented in an Abaqus User Element script to solve the non-linear problem.

At the initial time $t = 0$, the concentration of vacancies is taken to be uniform throughout the stress-free body

$$c_L(\vec{x},0) = c_L^0\,, \tag{76}$$

with $c_L^0 = 10^{-2}\,\mathrm{mol\,m^{-3}}$.

17

The vertical and horizontal displacements along the bottom and left edges respectively have been constrained in view of symmetry, while the top edge and the boundary of the hole have been regarded as traction-free, as depicted in Fig. 1. A linearly time-increasing displacement has been enforced along the Dirichlet right edge $\partial^D V = \partial^r V$

$$u_x(\vec{x}, t)|_{\partial^D V} = 0.02\,\overline{R}\,\frac{t}{t_{end}}\,, \qquad \forall t \in [0, t_{end}]\,. \tag{77}$$

The concentration of vacancies has been prescribed along the top ($\partial^t V$) and right ($\partial^r V$) edges following [43], i.e.

$$c_L(\vec{x}, t)|_{\partial^t V} = c_L(\vec{x}, t)|_{\partial^r V} = c_L^0\,, \qquad \forall t \in [0, t_{end}]\,. \tag{78}$$

The flux of vacancies across the boundary of the hole ($\partial^h V$) has been set to zero. The same applies to the bottom ($\partial^b V$) and left ($\partial^l V$) edges because of symmetry

$$\vec{h}_L(\vec{x}, t) \cdot \vec{n} = 0 \quad \vec{x} \in \partial^h V \cup \partial^b V \cup \partial^l V\,, \forall t \in [0, t_{end}]\,. \tag{79}$$

Several discretizations have been used in the numerical analyses. A mesh of 2400 elements is depicted in Fig. 1.

The hosting material, aluminum, is characterized by Young's modulus $E = 70\,\mathrm{GPa}$, Poisson's ratio $\nu = 0.34$ and yield stress $\sigma_Y = 200\,\mathrm{MPa}$. A negative value $\omega_L = -5 \times 10^{-7} \mathrm{m}^3\,\mathrm{mol}^{-1}$ has been taken for the chemical expansion coefficient, following [43]. From the same reference, it has been assumed a very high saturation limit for the vacancies $c_L^{max} = 10^5\,\mathrm{mol\,m}^{-3}$ and that the process occurs at constant temperature $T = 700\,\mathrm{K}$. The diffusivity is assumed $D_L = 10^{-8}\,\mathrm{m}^2\,\mathrm{s}^{-1}$.
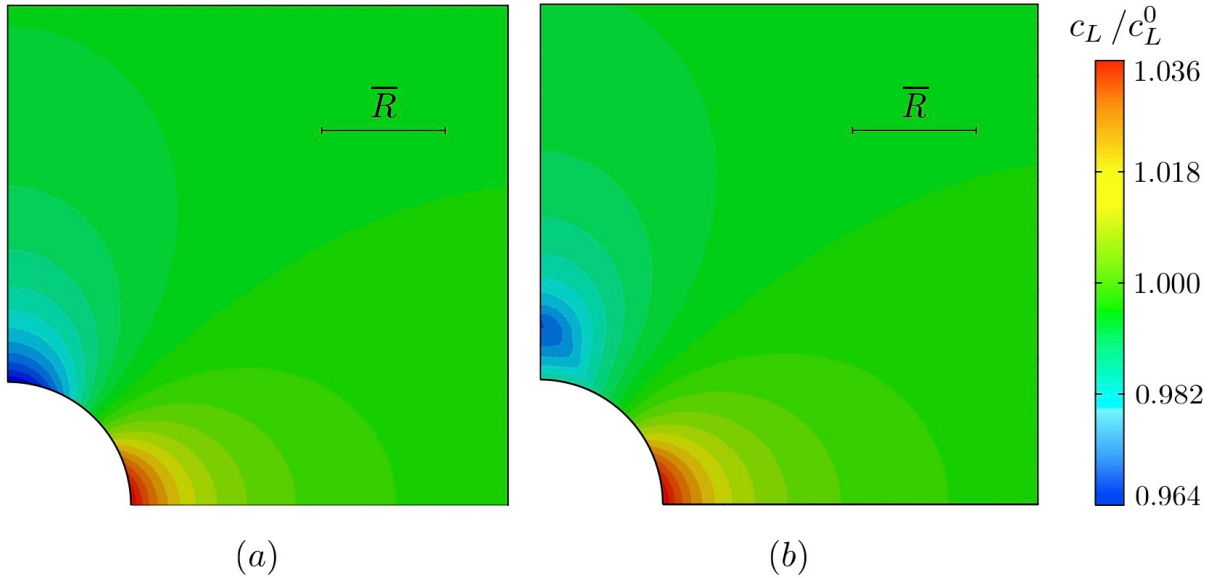
Figure 2: *Vacancies concentration at time $t = t_{end}$. a) Contour plot of the concentration distribution in an elastic material; b) steady state concentration distribution for elastic perfectly plastic material behavior.*

Fig. 2 plots the concentration of vacancies at $t = t_{end}$, normalized by c_L^0. Fig. 2a depicts the profile of concentration of vacancies in linear elastic materials. Red regions show an increase of concentration whereas the blue ones an opposite tendency. This distribution is consistent with Fig. 6 of [43]. The hydrostatic stress drives vacancy redistribution.

The role of the hydrostatic stress on vacancy distribution is analogous in EPP materials, yet differences arise in Fig. 2b. The decrease of concentration along the left edge is less pronounced and the location where
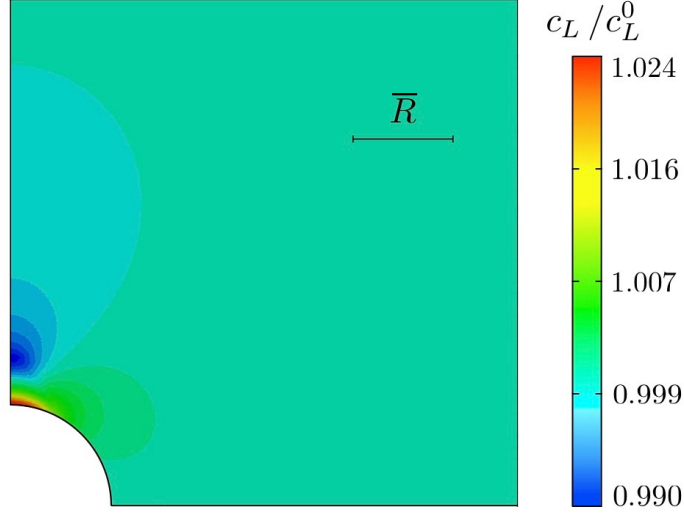
Figure 3: *Vacancies concentration. Contour plot of the steady state concentration distribution for elastic perfectly plastic material behavior after unloading.*

the minimum is attained is shifted along the edge. The different concentration configurations follow from different stress distribution, see also Fig. 4a.

The effect of a loading-unloading cycle on the distribution of vacancies has been studied and plotted in Fig. 3. The loading process has been taken from Eq. (77) and then reversed until condition $u_x|_{\partial^D V} = 0$ was restored. Plastic deformations persisted after unloading, see Fig. 3. A non-uniform distribution of vacancies was induced by the corresponding stress field, in agreement with Fig. 9 of [43].

Analytical expressions for the stress and concentration fields at steady state in coupled diffusion-*elasticity* problems are available in [43]. They are depicted in Fig. 4, in terms of hydrostatic stress and concentration distribution along the perimeter of the hole (where angles $\delta = 0°$ and $\delta = 90°$ correspond to the bottom and left edges, respectively).
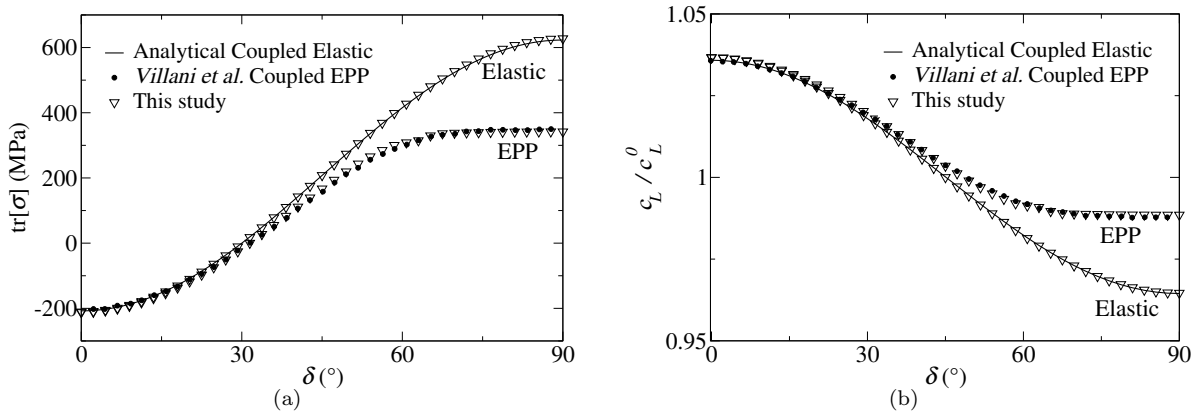
Figure 4: *Distribution of the hydrostatic stress and of the concentration of vacancies along the hole of the plate. The latter has been normalized by the initial concentration c_L^0. The analytical solution for the coupled elastic-transport problem is plot with a continuous line and compared to the outcomes of the numerical analyses in Villani et al. (dots) and of this contribution (triangles) at time $t = t_{end}$. EPP identifies the elastic perfectly plastic material behavior.*

The finite element approximation for the trace of the hydrostatic stress in elastic materials is excellent: it perfectly overlaps the analytical solution, see Fig. 4a. For an elastic perfectly plastic (EPP) material a

reduction of the stress gradient is visible for $\delta > 40°$, due to the Mises stress being limited by the yield stress σ_Y. The numerical approximation obtained with the present formulation is in perfect agreement with the numerical outcomes reported by Villani et al. [43], as depicted in Fig. 4a.

Note that stresses do not seem to be influenced by vacancy concentrations, since the swelling contribution is very small compared to the mechanical deformations.

Figure 4b shows the concentration profiles, predicted either analytically (Elastic) and numerically (Elastic and EPP), expressed in terms of the vacancy concentration normalized by c_L^0 along the surface of the hole. A good agreement has been found against the solution provided by [43]. Numerical results show deviations of the vacancy concentration from the initial value within a 5% range. As a consequence, $c_L \ll c_L^{max}$, which could be consistent with an infinitely dilute solution formulation.

7.2   H-embrittlement in metals

In modeling hydrogen embrittlement in metals within the thermodynamic framework we built, we keep some simplifying assumptions that are often taken in this field of research. On the unsatisfactory basis that there is insufficient information either from experiments or detailed micro mechanical models, it is for instance accepted that chemical expansion coefficients ω_L and ω_T are equal. Furthermore, since during hydrogen diffusion no significant phase changes seem to arise in steel, concentrations have little influence on its elastic properties and on the defect energy. Thermal equilibrium is here conjectured as in [2, 5, 6, 7, 17]. As a consequence, chemical potentials in eq. (93) simplify as follows:

$$\mu_\beta = \mu_\beta^0 + RT \ln[\frac{\theta_\beta}{1 - \theta_\beta}] \tag{80}$$

for $\beta = L, T$.

The hypothesis of *infinitely fast chemical kinetics* for trap filling is usually attributed to Oriani [2], who postulated that within a continuum-level material point the microstructure affects the local distribution of hydrogen, keeping the hydrogen in trapping sites in thermodynamic equilibrium with lattice sites. The concentrations of trapped species can be related to the interstitial one by equation (67), i.e.

$$\mu_L^0 + RT \ln[\frac{\theta_L}{1 - \theta_L}] = \mu_T^0 + RT \ln[\frac{\theta_T}{1 - \theta_T}] \, . \tag{81}$$

Taking into account definition (50) for the *equilibrium constant* K_{eq}, simple algebra leads from eq. (81) to

$$\theta_T = \left(1 + \frac{1}{K_{eq} \, \theta_L}\right)^{-1} \tag{82}$$

under the usually accepted assumption that $\theta_L \ll 1$. Equation (82) replaces the governing Eq.(68b).

Kumnick and Johnson [4] carried out permeation tests on pure iron with hydrogen gas charging and found that the trap density in iron increases sharply with deformations at low deformation levels and increases more gradually with further deformation. They also envisioned one single type of trap and estimated a trap binding energy $\Delta E_\tau = -60 \, \text{kJ mol}^{-1}$ independent of the deformation level within the range of $0 - 80\%$ cold work and independent on temperature within the range of $288 - 343$K. A fit of the number of trap sites vs equivalent plastic strain ε^p which is close to their experimental observations is

$$\log[c_T^{max} \, N_A] = 23.26 - 2.33e^{-5.5\varepsilon^p} \tag{83}$$

with N_A denoting Avogadro's number. After some manipulations, Eq.(68a) transforms into the following

$$\left[1 + \frac{c_T^{max}(\varepsilon^p)}{c_L^{max}} \, \frac{K_{eq}}{(1 + K_{eq}\theta_L)^2}\right] \frac{\partial c_L}{\partial t} + \theta_T \, \frac{\partial c_T^{max}}{\partial \varepsilon^p} \, \frac{\partial \varepsilon^p}{\partial t} - \text{div} \, [\, \mathbb{D}_L \, \nabla \, [\, c_L \,] - 3 \, \omega_L \, \boldsymbol{M}(c_L) \, \nabla \, [\, p \,]] = 0 \tag{84}$$

A fit of data from [4] was adopted by Sofronis and McMeeking [5] to account for the dependence of the number of traps on plastic deformation $c_T^{max}(\varepsilon^p)$. The term $\theta_T \frac{\partial c_T^{max}}{\partial \varepsilon^p} \frac{\partial \varepsilon^p}{\partial t}$ was introduced later by Krom et al. [6], who adopted (83) to follow the history variation of traps.

The diffusivity $\mathbb{D}_L = 1.27 \times 10^{-8} \, \text{m}^2 \, \text{s}^{-1}$, the chemical expansion coefficient $\omega_L = 6.67 \times 10^{-7} \text{m}^3 \, \text{mol}^{-1}$, the saturation limit for lattice population $c_L^{max} = 8.43 \times 10^5 \text{mol} \, \text{m}^{-3}$, as well as the standard Gibbs free energy change for the reaction $\Delta E_\tau = -60 \, \text{kJ} \, \text{mol}^{-1}$ have been chosen according to [5]. The equilibrium constant was determined to be $K_{eq} = 2.8 \times 10^{10}$ by making use of Eq.(50).

The Young's modulus $E = 207 \, \text{GPa}$, Poisson's ratio $\nu = 0.3$ and initial Yield stress $\sigma_{Y0} = 250 \, \text{MPa}$ were taken. The power-law hardening relationship adopted in [5] for the host material has been piecewise linearized, see Fig. 5.
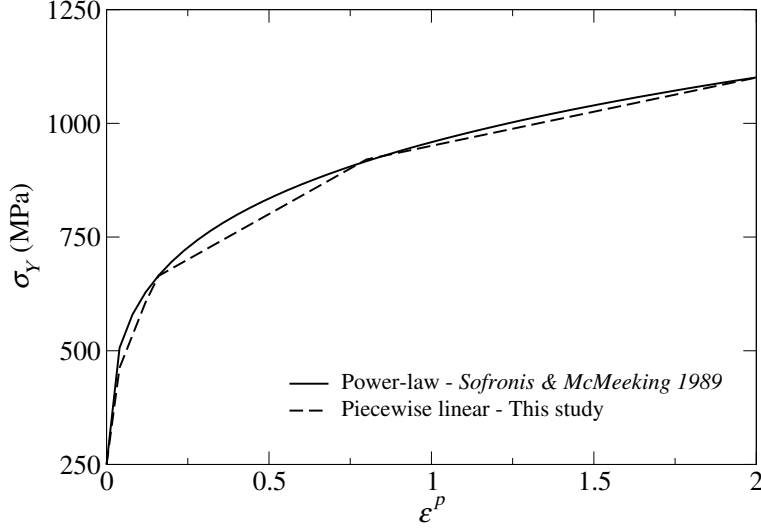
Figure 5: *Plot of the yield stress dependence on equivalent plastic strain. Comparison between the power law adopted in the literature [6, 5, 41] and the piecewise linear approximation adopted in the present contribution.*

7.2.1 Infinite plate with a circular hole

Consider the infinite plate with a circular hole analyzed in section 7.1 with a uniform concentration $c_L^0 = 3.46 \times 10^{-3} \text{mol} \, \text{m}^{-3}$ of hydrogen in the lattice which is in equilibrium with a trap population c_T^0 according to (82). The initially undeformed body is subject to a far field displacement, able to induce plastic deformations in the region nearby the hole, which generate new trap sites. The process leads to a redistribution of hydrogen both in the lattice and in the newly generated traps. The hole is insulated and boundary condition (79) holds, i.e. the surface insertion/extraction of hydrogen between the body and the environment is very slow compared to the speed of the redistribution of internal hydrogen due to diffusion coupled to mechanical stresses. Thermal equilibrium is enforced at $T = 300 \, \text{K}$.

The imposed displacements along the right edge have been tuned according to (77), adopting values of t_{end} ranging from 1 s to 100 s in order to investigate the effect of the strain rate. The surrounding part of the body is set to be a reservoir of hydrogen: the concentration is thus prescribed[8] according to (78). Boundary

---

[8]Although concentrations are widely imposed as Dirichlet boundary conditions, the latter should rather enforce the equilibrium between H$_2$ in the the environment and the lattice hydrogen [41] as an equivalence of chemical potentials:

$$\mu_L = \frac{1}{2} \, \mu_{H_2} \tag{85}$$

According to [41], the chemical potential μ_{H_2} can be expressed in terms of the fugacity f_{H_2} of the gaseous species and a reference pressure p^0:

$$\mu_{H_2} = \mu_{H_2}^0 + RT \, \ln \frac{f_{H_2}}{p^0} \tag{86}$$

The standard chemical potential $\mu_{H_2}^0$ conventionally vanishes at a pressure of 0.101MPa and at a temperature of 298K. Equation (85) thus leads to a non linear boundary condition of type:

$$RT \, \ln \frac{c_L}{c_L^{max} - c_L} - 3\omega_L \, p = \frac{\mu_{H_2}^0}{2} - \mu_L^0 + RT \, \ln \sqrt{\frac{f_{H_2}}{p^0}} \qquad \vec{x} \in \partial^D V \tag{87}$$

.

conditions (79) have been applied on the remaining edges.

Figure 6a shows the behavior of the hydrostatic stress and the concentration divided by the initial value along the boundary of the hole ($\delta = 0°$ and $\delta = 90°$ respectively indicate bottom and left edges). It is worth noticing that the distribution of lattice concentration is reversed with respect to section 7.1 which is expected in view of the positiveness of ω_L. The non-symmetric profile of concentration agrees with the distribution of vacancies in aluminum when the elastic perfectly plastic material behavior was considered.

Figure 6b shows the distribution of the equivalent plastic strain ε^p, trap concentration c_T and saturation limit c_T^{max} along the boundary of the hole. Concentrations have been normalized by c_L^0. The number of traps increases by 50% on the upper part of the hole, where plastic deformations occur, in agreement with Eq.(83). Traps sites are close to the saturation limit ($\theta_T \sim 0,99$), in agreement with constraint (82).

Numerical analyses have been carried out at different strain rates. No major differences in either c_L or c_T distributions have been observed (Fig. 6b refers to the outcomes obtained for $t_{end} = 100$ s), since the deformation induced by the boundary conditions is not sufficiently large to induce a depletion of the lattice sites in favor of traps.
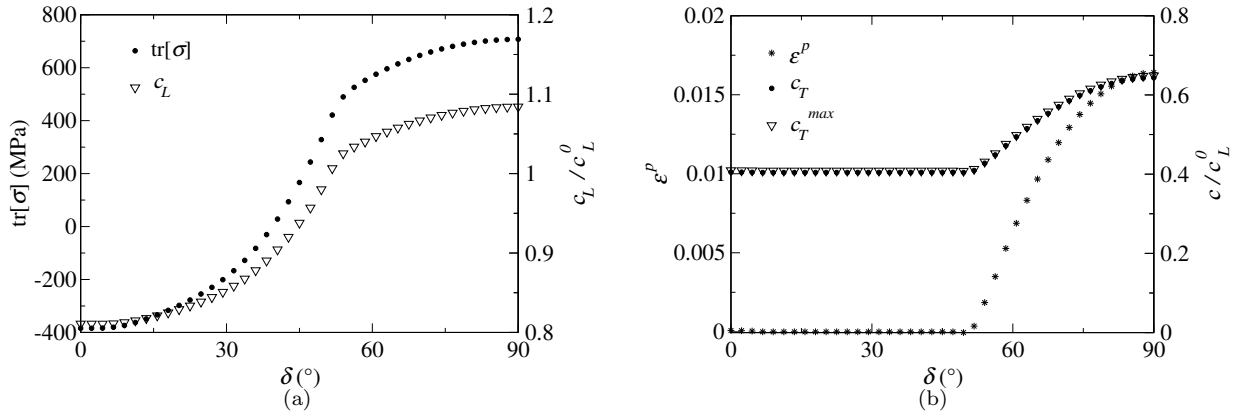

Figure 6: *Two dimensional plots of a) hydrostatic stress and lattice concentration and b) equivalent plastic strain together with trap concentration and trap saturation limit along the hole of the plate. All the concentration distributions have been normalized by the initial lattice concentration c_L^0. The plots refer to the last step of increment of load, $t_{end} = 100$ s*

7.2.2 Diffusion at a blunted crack tip.

A specimen containing a small blunted crack tip is considered, as in Fig. 7. It is embedded in a gaseous hydrogen environment at pressure $p_{H_2} = 1$ atm and temperature $T = 300$K. The latter does not change during the whole process. The specimen has an initial uniform interstitial hydrogen content $c_L^0 = 3.46 \times 10^{-3}$ mol m^{-3}. A plane strain, local yielding configuration is enforced - as in [5] - by choosing a small crack tip radius, negligible if compared to the specimen characteristic length. In this way, the small scale yielding conditions are satisfied, i.e. the plastic zone is confined in an annular area about the crack tip whose size is negligible compared with any dimensions of the specimen. The boundary of the annulus is subjected to a given displacement field

$$u_x\left(\overline{R}, \delta\right) = \frac{K_I}{2\,\mu}\sqrt{\frac{\overline{R}}{2\,\pi}}\,\cos\left(\frac{\delta}{2}\right)\left[2 - 4\nu + 2\,\sin^2\left(\frac{\delta}{2}\right)\right] \tag{88}$$

$$u_y\left(\overline{R}, \delta\right) = \frac{K_I}{2\,\mu}\sqrt{\frac{\overline{R}}{2\,\pi}}\,\sin\left(\frac{\delta}{2}\right)\left[4 - 4\nu - 2\,\cos^2\left(\frac{\delta}{2}\right)\right]$$
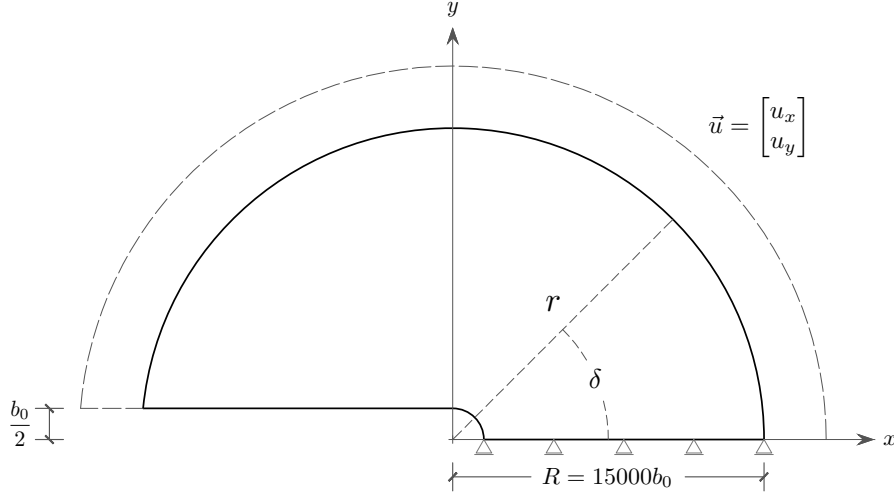
22

Figure 7: *Schematic of the blunted crack geometry and boundary conditions. The initial crack tip opening displacement is b_0 and the external radius of the domain used in numerical analyses is R. Following [6, 5, 41], the diameter of the notch is $b_0 = 10\,\mu m$ and the outer radius is $\overline{R} = 15000\,b_0$.*

which induces a tensile Mode-I loading [5]. In Eq.(88) K_I is the stress intensity factor obtained from the linear elastic crack problem *at the specimen length-scale*. K_I is linearly increasing in time

$$K_I(t) = \tilde{K}_I \, \frac{t}{t_{end}} \quad t \in [0, t_{end}] \tag{89}$$

where $\tilde{K}_I = 89,2\,\mathrm{MPa\,m^{-1/2}}$ and $t_{end} = 130\,\mathrm{s}$. Displacements along the y direction have been constrained along the symmetry axis while the crack surface has been modeled as traction-free, see Fig. 7.

In order to compare our results with [6], the contributions of the pressure and of the saturation of c_L are neglected in boundary condition (87), while the fugacity equals the external pressure, exploiting the ideal gas model. In this way the lattice concentration at the external boundary coincides with the initial value inside the specimen. Its numerical value is computed from Sievert's law:

$$c_L = K_s \, \sqrt{p_{H_2}} \, \exp\left(\frac{-\overline{\Delta H}}{R\,T} \right) \tag{90}$$

where the experimentally measured constants K_s, $\overline{\Delta H}$ hold [5]:

$$K_s = 1040 \frac{\mathrm{mol}}{\sqrt{\mathrm{MPa}\,\mathrm{m^3}}} \qquad \overline{\Delta H} = \mu_L^0 = 28.6 \frac{\mathrm{KJ}}{\mathrm{mol}} \tag{91}$$

The initially uniform concentration $c_L^0 = 3.46 \times 10^{-3}\,\mathrm{mol\,m^{-3}}$ is computed from (90) at $T = 300\,\mathrm{K}$ and $p_{H_2} = 1\,\mathrm{atm}$. A uniform initial concentration c_T^0 is established in view of equilibrium condition (82). Lattice concentration $c_L = c_L^0$ has been prescribed along the outer radius and the crack surface to simulate a process in which the reaction kinetics with the environment is fast compared to the diffusion rate of the hydrogen Along the symmetry axis the hydrogen flux has been set to zero.

23

The mesh consists of approximately 1200 elements (about 60 and 20 along the radial and tangential direction respectively) biased from the notch across the annulus.

Figure 8 plots the pressure distribution as well as the equivalent plastic strain ε^p in proximity of the blunted crack tip along symmetry axis x. Coordinate x has been normalized to the *nominal crack-tip opening displacement* $b = 4.7\,b_0$ following [6]. Plots refer to time $t = 130\,\mathrm{s}$.
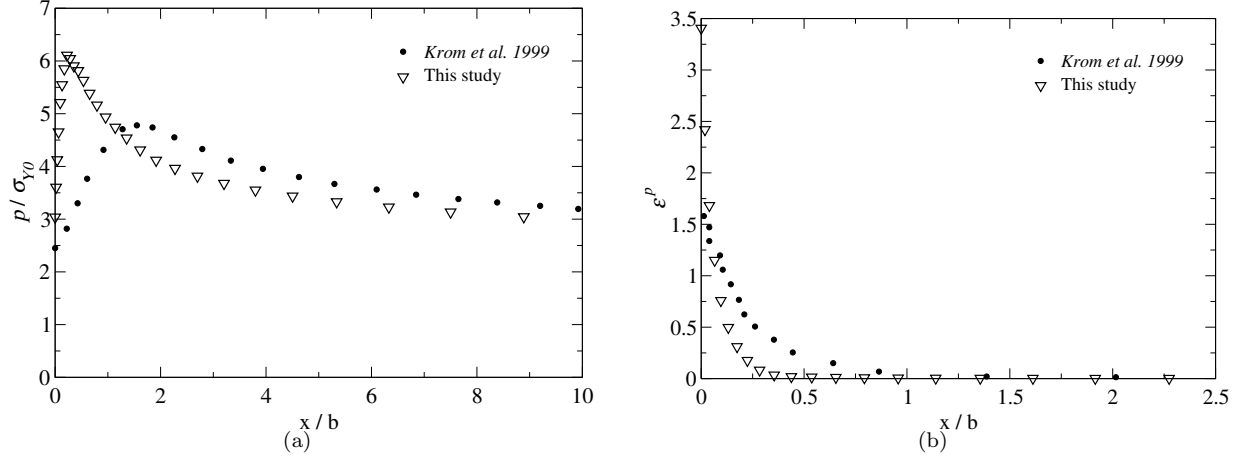

Figure 8: *(a) Pressure divided by the initial yield stress σ_{Y0}; (b) Equivalent plastic strain in proximity of the crack tip along the symmetry axis (two different scales have been used for the x-axis). The plots show a comparison between numerical analyses carried out in this work and the results of Krom et al. [6] referring to the final step of load application, $t = 130\,\mathrm{s}$.*

A comparison with the results of Krom et al. [6] is made. An overestimation of the pressure and a shift of the peak is shown. The maximum predicted equivalent plastic strain roughly doubles the one predicted by Krom et al.. These differences are due to the hypothesis of small deformations, that severely influences the outcomes around the crack tip. The value of the equivalent plastic strain in Fig. 6b and Fig. 8b differ by two orders of magnitude, which shows the different impact on trap generation in the two examples.
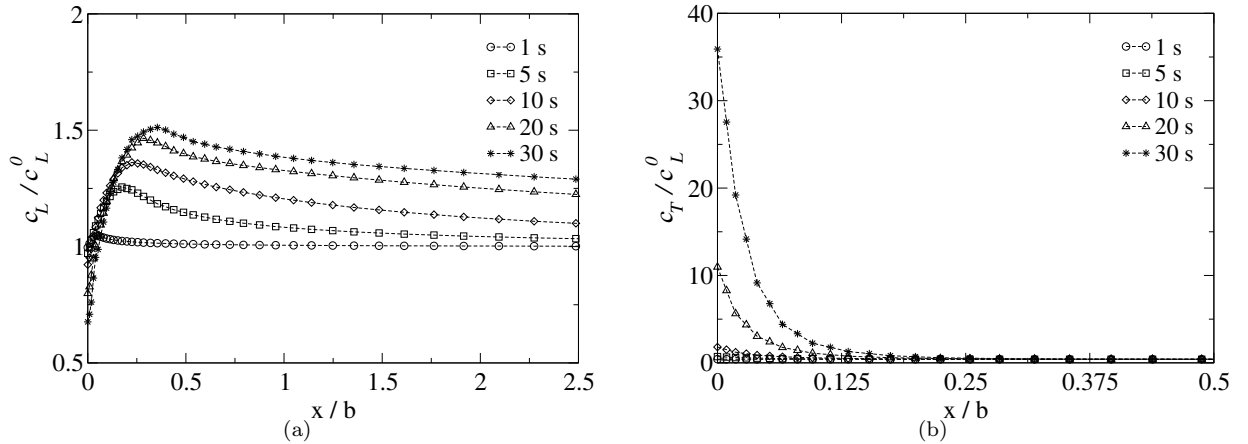

Figure 9: *Plot of lattice (a) and traps (b) concentration normalized to the initial lattice concentration c_L^0 in proximity of the crack tip for different instants of time during the loading process (two different scale have been used for the x-axis).*

Figure 9 shows the distribution of concentrations c_L and c_T along the symmetry axis at different times. An increase of trap concentration is limited to a narrow zone across the crack tip, in agreement with the

development of plasticity predicted by the small strain theory, Fig. 8b. A depletion of concentration in the lattice follows.

It can thus be concluded that the assumption of small strains should be questioned for the evaluation of strains and stresses in the vicinity of the crack tip (although blunted), since it may induce significant errors. This interesting conclusion strengthens the motivation for the extension of the present formulation to finite strains, which is in progress and will be the subject of further publications.

7.3   Li-ion insertion in storage particles

The functioning of battery cells entails a series of multi-physics and chemistry processes [37, 44, 45, 46, 47, 48]. A recent review can be found in [49]. Here we study the insertion of ionic lithium in active particles within battery cells.

When the host material has layer-type crystal structures there is space available for the presence of small ionic species such as Li^+ cations [50]. Lithium Cobalt Oxide ($LiCoO_2$) is one of these materials. It has been studied for almost 40 years [51], showing excellent properties which make it widely used as a cathode material for commercial applications.

Depending upon the lithium content, the mobile species in $LiCoO_2$ can randomly occupy sites between the layers (the so-called galleries) or may cause a modification of the host structure. In the former case, transient concentration gradients take place in the gallery space, whereas during phase-transitions the insertion process involves the motion of an interface that separates the Li-poor from the Li-rich regions. Lithium diffusing in galleries (here thought of as interstitially) will be denoted Li_L hereafter and its concentration c_L. When the insertion or extraction of ionic species causes changes in the structure of the host materials, some Li_L becomes immobile, because it is trapped in a different host crystal structure. The trapped lithium will be denoted henceforth Li_T and its concentration c_T.

These events alter the material properties of the lithiated phase with respect to the pristine material, inducing a significant change in volume of the host particle with consequent generation of a stress field, which in turn influences the reaction kinetics and the mass transport. As described extensively in [44, 52, 53], the driving force for these phenomena is the jump in the electrochemical potential at the boundary of the particles, the location where they meet the electrolytic solution. Since this example intends to illustrate merely the effects of trapping, a rigorous treatment of Butler-Volmer boundary conditions is deferred to other publications [54].

Mechanical effects induced by phase changes are captured by the dissipation potential and by the evolution of the elastic part of the free energy with trapped and interstitial concentrations ($\partial\psi_{el}/\partial c_T$ and $\partial\psi_{el}/\partial c_L$). The latter is usually negligible and in the present case-study the influence of trapping on the free energy as well as the energy interactions are neglected, too. We thus assume

$$\frac{\partial\psi_{el}}{\partial c_L} = 0 , \qquad \frac{\partial\psi_{el}}{\partial c_T} = 0 , \qquad \chi = 0 . \tag{92}$$

The simplifying assumption of thermal equilibrium will be taken here, i.e. no thermal evolution and runaway is here accounted for. These assumptions will be removed within a specialized publication, which is currently in progress. As a consequence, chemical potentials in eq. (93) simplify as follows:

$$\mu_\beta = \mu_\beta^0 + RT \ln[\frac{\theta_\beta}{1 - \theta_\beta}] + \frac{\partial\psi_{in}}{\partial c_\beta} . \tag{93}$$

The stress state evolves with the inelastic deformations, driven by the concentration of trapped species c_T through the following visco-plastic law of Perzyna type:

$$\frac{\partial\boldsymbol{\varepsilon}^{in}}{\partial t} = \frac{\text{dev}\,[\,\boldsymbol{\sigma}\,]}{||\,\text{dev}\,[\,\boldsymbol{\sigma}\,]\,||}\,\gamma , \qquad \gamma = g(\theta_T)\,\sqrt[m]{\varphi^{in}}\,\mathcal{H}(\varphi) \tag{94}$$

In Eq.(94) the Mises yield function φ^{in} described by Eq. (75) is used. It was concluded in [55] that the flow stress of lithiated silicon decreases as the Li concentration increases: the concentration of trapped lithium influences therefore the yield strength σ_Y of silicon, whose evolution is governed by internal variables related to a defect energy ψ_{in}. To the best of our knowledge, there are no similar experimental data for $LiCoO_2$ and thus no hardening is assumed henceforth, i.e.

$$\psi_{in} = 0 . \tag{95}$$

Again in Eq.(94): $m > 0$ is a rate-sensitivity parameter; $\mathcal{H}$ is the Heaviside step function; $g(\theta_T)$ is a given function of the concentration of trapped species, which fuels the visco-plastic flow. A simple choice for $g(\theta_T)$ is the linear function:

$$g(\theta_T) = g_0\,\theta_T \tag{96}$$

with g_0 a given positive parameter. Flow-rule (94) is clearly associated, and satisfies Clausius-Planck inequality (31) in view of plastic incompressibility.

The process of trapping is modeled by the finite speed chemical kinetics Eq.(62a). In view of all the assumptions made above, it holds from Eq. (62b,c):

$$k_L = \tilde{k}_L\,, \qquad k_T = \tilde{k}_T\,.$$

Material parameters have been selected for $LiCoO_2$ - from [9, 56] - and made dimensionless using the time scale $\bar{t} = 1\,s$, the length scale $\overline{L} = 10\,\mu m$, the concentration scale $\bar{c} = 5.16 \times 10^4\,mol\,m^{-3}$, and the stress scale $\bar{\sigma} = 10\,GPa$. The selected non-dimensional parameters and their numerical values are listed in Table 1. For paucity of space, only the influence of the two chemical parameters, i.e. K_{eq} and $\tilde{k}_L$, is investigated in promoting the trapping process and modifying the overall response. The dimensionless amount $\overline{k}_L$ is defined as

$$\overline{k}_L = \tilde{k}_L\,\bar{t}/c_L^{max}$$

Parameter	Value	Parameter	Value
$\mathbb{D}_L\,\bar{t}/\overline{L}^2$	1.00	$RT\,c_L^{max}/G$	0.52
K_{eq}	300	$G/\bar{\sigma}$	1.00
$\overline{k}_L$	$0.01 \div 100$	K/G	2.17
$c_L^{max}/\bar{c}$	1.00	σ_Y/G	0.15
c_T^{max}/c_L^{max}	0.20	$g_0\,\bar{t}\,G^{\frac{1}{m}}$	12.41
$\omega_L\,\bar{\sigma}/(RT)$	0.03	m	5
$\omega_T\,\bar{\sigma}/(RT)$	0.17		

Table 1: *Non-dimensional parameters used in our numerical example. Parameters R and T stand for the gas constant and absolute temperature respectively.*

A spherical particle V of unit radius $r/\overline{L} = 1$ is considered. It is initially empty of lithium ($c_L(\vec{x}, t = 0) = c_T(\vec{x}, t = 0) = 0$) and undeformed ($u(\vec{x}, t = 0) = 0$). The particle is free to expand at its boundary, i.e. $\partial V = \partial^N V$ and $\boldsymbol{\sigma}(\vec{x}, t)\,\vec{n}(\vec{x}) = \vec{0}$ on $\vec{x} \in \partial^N V$ for all t. Furthermore, galvanostatic boundary conditions on mass flux $\vec{h}_L(\vec{x}, t) \cdot \vec{n}(\vec{x}) = \frac{\bar{c}\overline{L}}{\bar{t}}\,\overline{h}$ are imposed on $\vec{x} \in \partial V$. Scalar $\overline{h}$ is defined as follows:

$$\overline{h} = \begin{cases} 1/2 & \text{if } \theta_L(\vec{x} \in \partial V, t) <= 0.4 & (a) \\ 0 & \text{until equilibrium} & (b) \\ -1/2 & \text{until } \theta_L(\vec{x} \in \partial V, t) = 0 & (c) \end{cases} \tag{97}$$

Accordingly, in a first stage the particle is lithiated until the lattice concentration on the boundary reaches 40% of saturation. The particle reaches an equilibrium configuration afterwards. Eventually lithium is extracted until no interstitial lithium remains at the boundary.

The set of boundary conditions above configures a spherical symmetric solution $c_L(r), c_T(r), u(r)$. The governing equations have thus been restated in a spherical coordinate system $\{r, \vartheta, \phi\}$ centered at the centroid of the sphere:

$$\frac{\partial c_L}{\partial t} + \frac{\partial h_r}{\partial r} + 2\frac{h_r}{r} + w^{(1)} = 0 \tag{98a}$$

$$\frac{\partial c_T}{\partial t} - w^{(1)} = 0 \tag{98b}$$

$$\frac{\partial \sigma_r}{\partial r} + 2\frac{\sigma_r - \sigma_\vartheta}{r} = 0 \tag{98c}$$

having defined

$$\boldsymbol{\sigma} = \sigma_r \ \vec{e}_r \otimes \vec{e}_r + \sigma_\vartheta \ (\vec{e}_\vartheta \otimes \vec{e}_\vartheta + \vec{e}_\phi \otimes \vec{e}_\phi) \tag{99}$$

$$\vec{h}_L = h_r \ \vec{e}_r \tag{100}$$

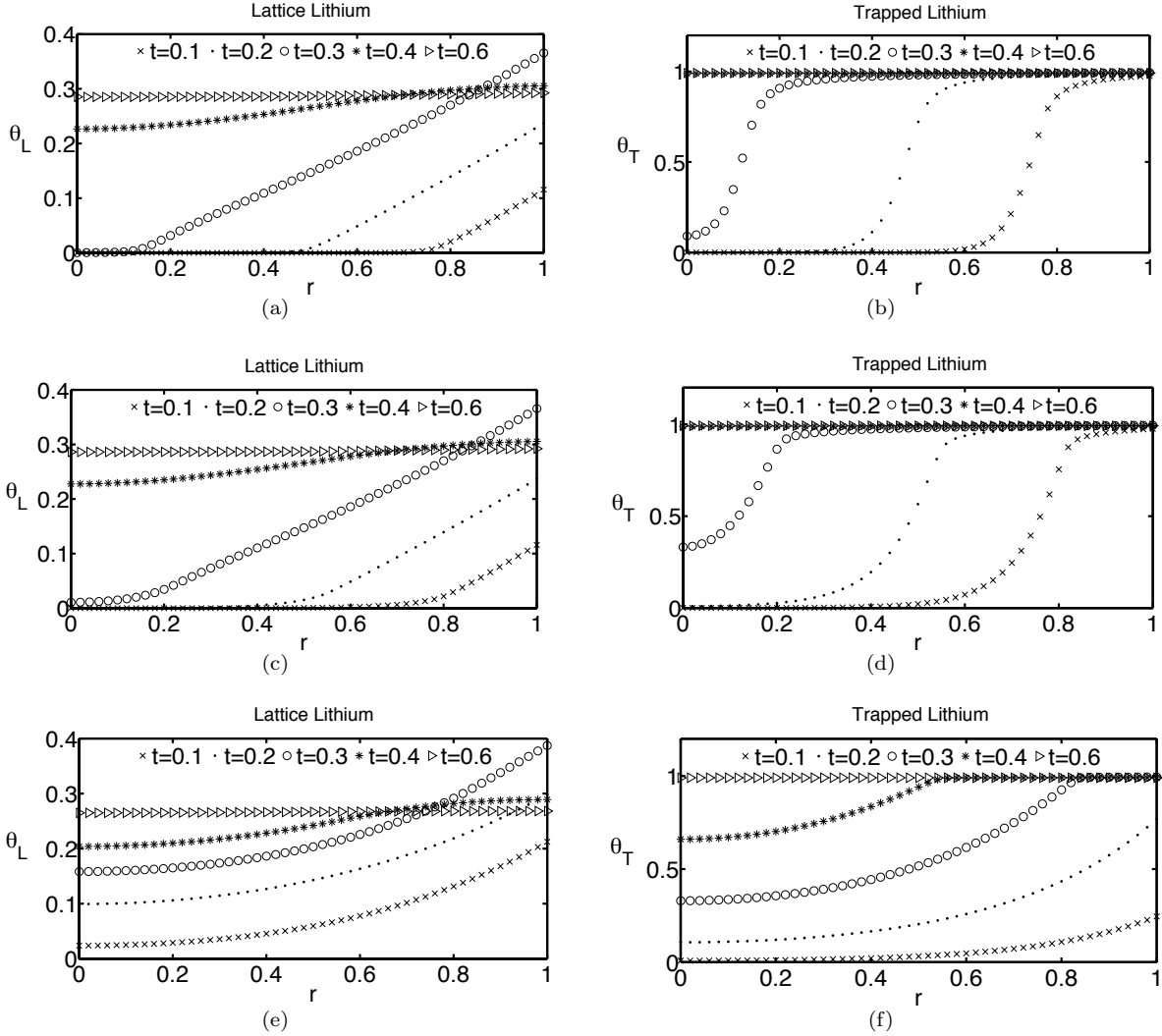Motion has been restrained by imposing a null displacement at the center of the particle, at $r = 0$.

Figure 10: *Distributions of the interstitial (a, c, e) and trapped (b, d, f) lithium at different times during insertion and subsequent zero influx conditions. In (b,d) all curves after $t = 0.4$ overlap. All the plots refer to an equilibrium constant $K_{eq} = 300$. (a,b) refer to an infinitely fast kinetics, whereas (c,d) to $\bar{k}_L = 1$ and (e,f) to $\bar{k}_L = 0.01$.*

Fig. 10(a,b) plot the distribution of interstitial and trapped lithium during insertion (condition (97a)) and subsequent zero influx (condition (97b)) for an equilibrium constant $K_{eq} = 300$ and infinitely fast kinetics. During insertion, the interstitial lithium diffuses with a basically constant gradient in space nearby the boundary ($r = 1$). The concentration drops down to zero subsequently, in a zone where the trapping reaction takes place. The trapped lithium tends to saturate ($\theta_T = 1$) in a zone close to the boundary, which

27

suggests that trapping reaction (1) has been completed. The concentration drops down to zero in the same zone for the interstitial lithium.

The concentration landscape identifies two phases in the host material, lithiated and pristine, separated by a gradient of concentration c_T in a localized zone, where the trapping reaction is taking place. The size of this zone is determined by the relative contributions of diffusion and reaction, through the values of the diffusivity $\mathbb{D}_L$ and the reaction constants k_L and k_T: fast and highly favored forward reaction (i.e. high equilibrium constant K_{eq}) causes strong phase segregation. Plots (c,d) hold for $\overline{k}_L = 1$, whereas (e,f) for $\overline{k}_L = 0.01$. The influence of the fast kinetics is evident. The gradient of concentration for c_T can be further increased by modifying the diffusivity at infinitely fast kinetics. Due to paucity of space, this and other analyses will be presented in a forthcoming, specialized publication.

The stored lithium cannot increase under condition (97b). Fig. 10 confirms that the concentration redistributes toward a configuration with interstitial and trapped lithium in thermodynamic equilibrium, which is numerically reached at 0.6 dimensionless time units. During current reversal, see Fig. 11, the extraction of the trapped lithium is slower and in a limit case might be even hindered by an extremely high trapping energy. Trapped lithium may remain in thermodynamic equilibrium with a small interstitial counterpart. This behavior suggests that alloying is included among the origins of first cycle capacity loss, observed experimentally in some compounds [13, 57], since the inserted lithium may not be fully extracted.
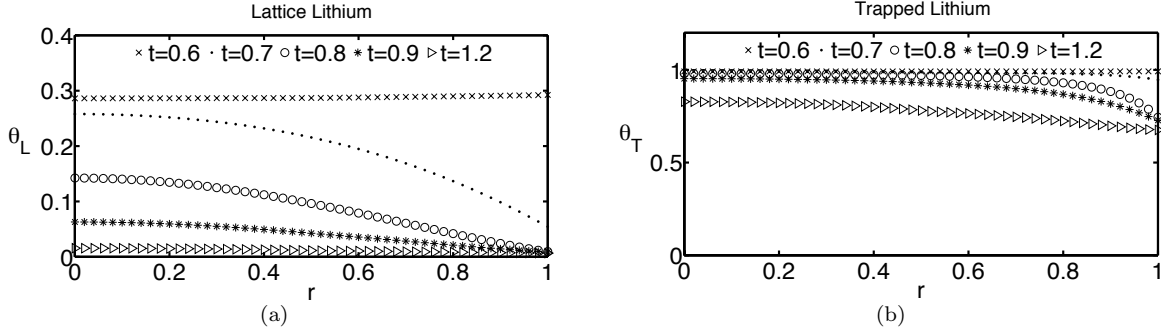

Figure 11: *Distributions of the interstitial (a) and trapped (b) lithium at different times during extraction, beginning from the conditions at $t = 0.6$ of Fig. 10. All the plots refer to an equilibrium constant $K_{eq} = 300$ and $\overline{k}_L = 1$.*

Fig. 12(a,c) show that the radial stress evolves from an initial tensile state to a final compressive one under conditions (97a,b) and fast kinetics. At the beginning of lithiation, the swelling of the outer shell induces radial tension in the whole particle. Once the exterior part of the particle is fully saturated by trapped lithium, it inhibits further expansion of the inner core, which is swelling in the reaction zone. This new phenomenon induces a change in the radial stress state of the particle. At slow kinetics, the diffusion dominates inducing smooth concentration profiles that inhibits the stress overturn - see Fig. 12(e).

An inverse path is taken by the hoop stress at the boundary ($r = 1$), which evolves from an initial compression (due to the core-restraint to the outer shell volumetric expansion after the initial lithiation) to a tensile state after the saturation of the outer shell, as shown in Fig. 12(b,d). This change in the stress state, which explains the observed crack initiation from the outer boundary of the particles, has been discovered and discussed for silicon particles in [58, 59]. Fig. 12(f) shows that, remarkably, no change in sign is observed for the hoop stress at low kinetics.

Finally, no significant changes in the stress profile are seen upon lithium extraction, as plotted in Fig. 13.

Under the simulation conditions (97a,b) the radial plastic strain develops in the external half of the particle only, as it can be seen in Fig. 14(a), and only at fast kinetics since Fig. 14c clearly shows that no plastic strains develop. The deviatoric stress, proportional to the amount $\sigma_r - \sigma_\theta$ depicted in Fig. 14(b, d), shows that the plastic strain at a point $\vec{x}$ accumulates in a limited amount of time, which basically corresponds to the transit of the front of the lithiated zone through point $\vec{x}$. After saturation, no further
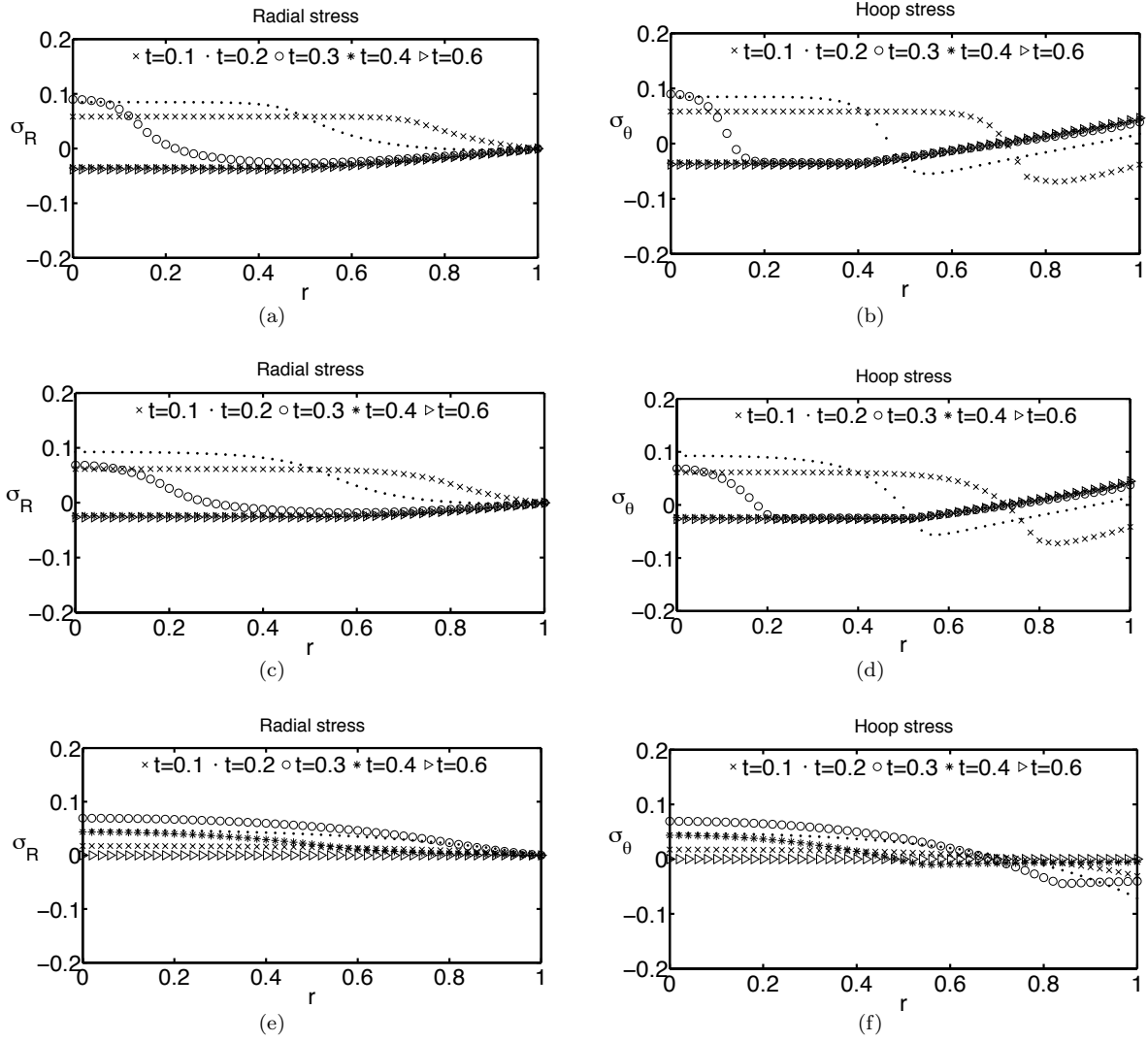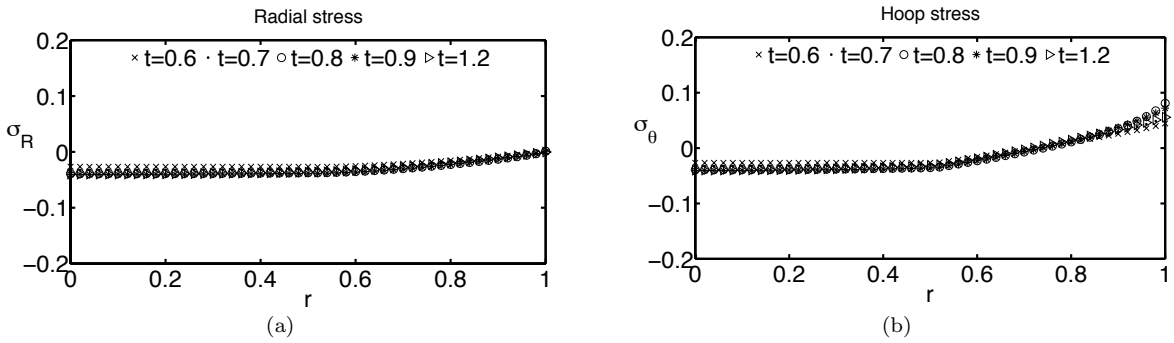
Figure 12 plots:

(a) Radial stress — ×t=0.1 ·t=0.2 ◦t=0.3 *t=0.4 ▷t=0.6; axes σ_R vs r

(b) Hoop stress — ×t=0.1 ·t=0.2 ◦t=0.3 *t=0.4 ▷t=0.6; axes σ_θ vs r

(c) Radial stress — ×t=0.1 ·t=0.2 ◦t=0.3 *t=0.4 ▷t=0.6; axes σ_R vs r

(d) Hoop stress — ×t=0.1 ·t=0.2 ◦t=0.3 *t=0.4 ▷t=0.6; axes σ_θ vs r

(e) Radial stress — ×t=0.1 ·t=0.2 ◦t=0.3 *t=0.4 ▷t=0.6; axes σ_R vs r

(f) Hoop stress — ×t=0.1 ·t=0.2 ◦t=0.3 *t=0.4 ▷t=0.6; axes σ_θ vs r

Figure 12: *Radial (a, c, e) and hoop (b, d, f) stresses during insertion and subsequent zero influx conditions. In (a-d) all curves after $t = 0.4$ overlap. All the plots refer to an equilibrium constant $K_{eq} = 300$. (a,b) refer to an infinitely fast kinetics, whereas (c,d) to $\overline{k}_L = 1$ and (e,f) to $\overline{k}_L = 0.01$.*

Figure 13 plots:

(a) Radial stress — ×t=0.6 ·t=0.7 ◦t=0.8 *t=0.9 ▷t=1.2; axes σ_R vs r

(b) Hoop stress — ×t=0.6 ·t=0.7 ◦t=0.8 *t=0.9 ▷t=1.2; axes σ_θ vs r

Figure 13: *Radial (a) and hoop (b) stresses at different times during extraction, beginning from the conditions at $t = 0.6$ of Fig. 12. All the plots refer to an equilibrium constant $K_{eq} = 300$ and $\overline{k}_L = 1$.*
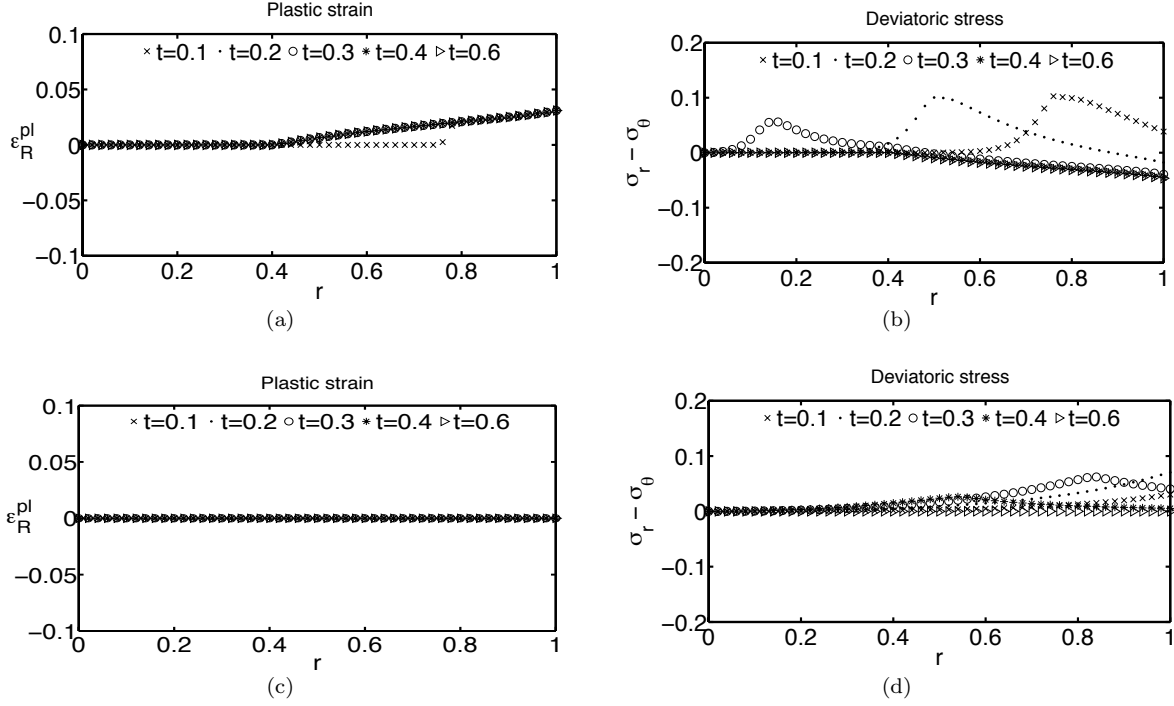
29

Figure 14: *Plastic strain (a, c) and deviatoric stress (b, d) during insertion and subsequent zero influx conditions. The dimensionless yield stress is $\sigma_y = 0.1$. In (a) all curves after $t = 0.2$ overlap. All the plots refer to an equilibrium constant $K_{eq} = 300$. (a,b) refer to an infinitely fast kinetics, whereas (c,d) to $\overline{k}_L = 0.01$. Outcomes at $\overline{k}_L = 1$ do not differ from infinitely fast kinetics and have not been reported.*

plasticity occurs. Fig. 14b also shows that at a given time most of the particle during lithiation remains in an elastic state, apart from a localized area where the reaction rate attains its maximum (compare with Fig. 16a). In the Li-trapped phase, the strains are dominated by the swelling contribution $\omega_T \left(c_T - c_T^0 \right)$, as depicted in Fig. 15. Elastic strains develop throughout the whole particle during the lithiation process.

During lithium extraction at $\overline{k}_L \leq 1$ no alteration of the plastic strain field takes place. The deviatoric stress undergoes small changes near the boundary, resembling the hoop stress evolution in Fig. 13, but seems of minor interest.

Figure 16 details the evolution in time of the reaction rate $w^{(1)}$. At infinitely fast kinetics, the reaction rate has a peak in a relatively narrow zone, which identifies an interphase that separates the lithiated and pristine phases - compare Figs. 16a and 10b. Such an interphase moves rapidly from the boundary to the core. When the kinetics is bounded but high, a similar behavior manifests, with a lower peak and a broader interphase - see Figs. 16b and 10d. When diffusion dominates, a different overall behavior arises. A narrow zone of steep gradient remains present, which slowly moves towards the center of the particle. In its wake towards the outer shell $w^{(1)}$ is negligible. In its front, the reaction rate is spread in a broad zone, in contrast with the reaction-dominated cases. During lithium extraction no evidence of a strong interphase arises, and the reaction rate is widespread in the whole particle.

Figure 17 plots the evolution in time of the equilibrium constant (63). The influence of the pressure is evident, but it is overall not particularly significant.

8   Concluding remarks

A continuum coupled model of transport-reaction-thermo-mechanics with trapping has been dealt with in this paper. It describes interstitial motion of guest species in a hosting material, with point-wise traps of
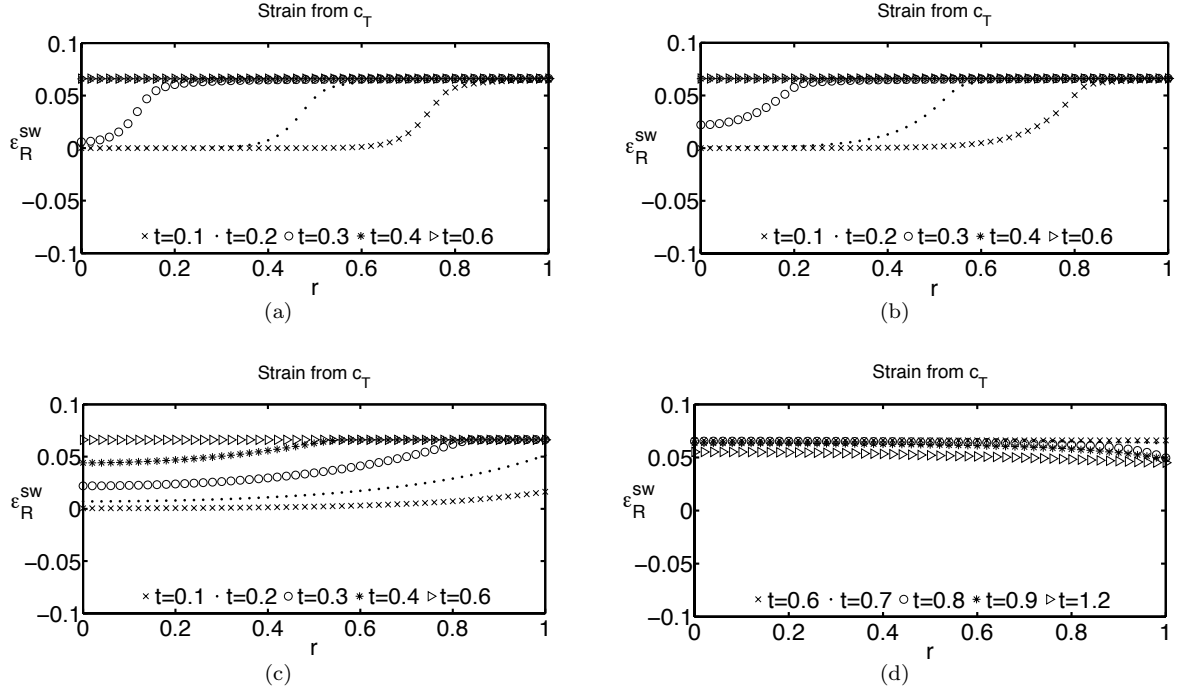
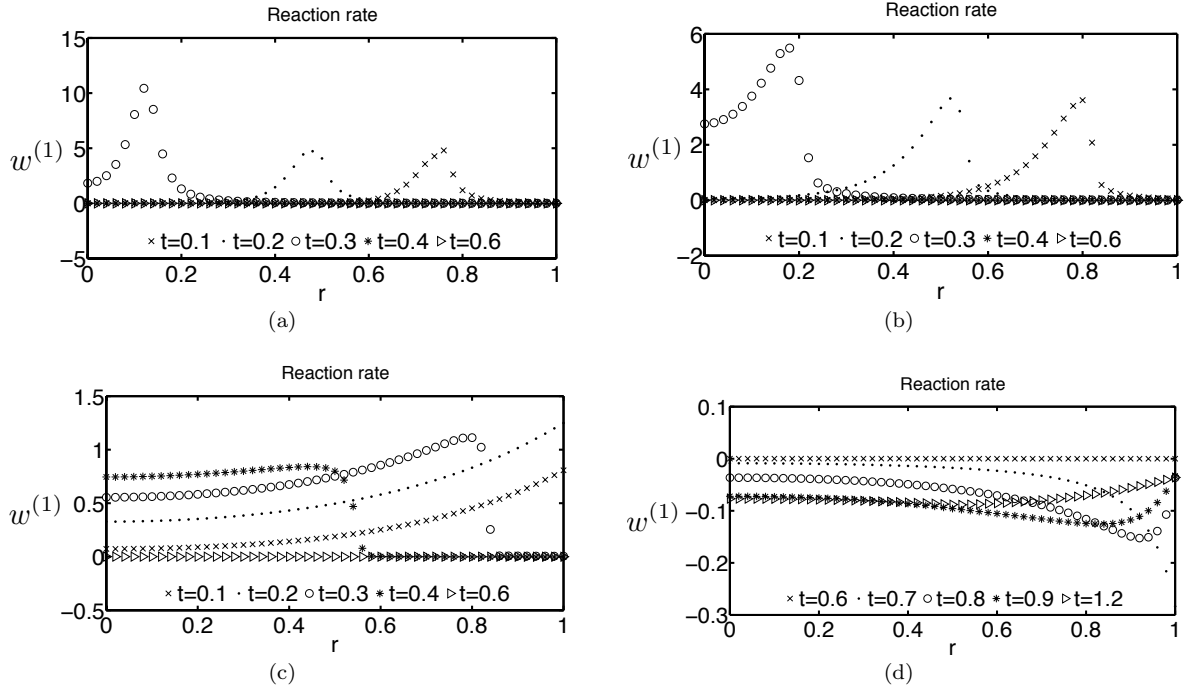Figure 15: *Swelling strain* $\omega_T \left(c_T - c_T^0\right)$ *during insertion and subsequent zero influx conditions (a-c) and during delithiation (d). All the plots refer to an equilibrium constant* $K_{eq} = 300$. *(a) refers to an infinitely fast kinetics, whereas (b,d) to* $\overline{k}_L = 1$ *and (c) to* $\overline{k}_L = 0.01$.

Figure 16: *Reaction rate during insertion and subsequent zero influx conditions (a-c) and during delithiation (d). All the plots refer to an equilibrium constant* $K_{eq} = 300$. *(a) refers to an infinitely fast kinetics, whereas (b,d) to* $\overline{k}_L = 1$ *and (c) to* $\overline{k}_L = 0.01$.
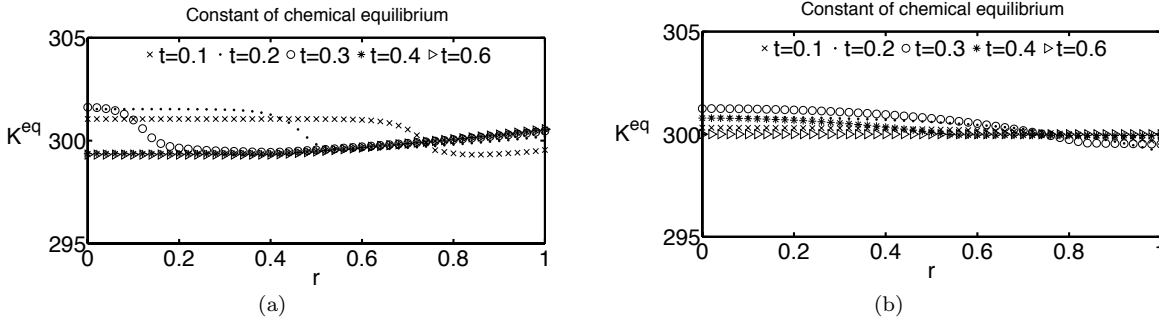
Figure 17: *Equilibrium constant during insertion and subsequent zero influx conditions. (a) refers to an infinitely fast kinetics, whereas (b) to $\overline{k}_L = 0.01$.*

generic type, their kinetics of filling and emptying, influenced by the mechanical stress state and by the temperature evolution.

The model is framed in standard thermodynamics [21]. The energy and entropy contributions of the mass flux in the balance equations are accounted for. The selection of the Helmholtz free energy and of the dissipation potential leads to different constitutive characterizations, which apply well to several multi-physics problems. In this regard, this manuscript can be compared to other papers devoted to specific problems. We used some terminology that differs from the definitions that usually appear in thermodynamic functions - see section 3.6 or the definition of chemical potential, for instance. In view of these original features and focusing on infinitesimal deformations we provided thorough derivations, differing advection to a companion paper. Similar reasoning holds for the analysis of mechanical failure [60, 61, 62, 63, 64], of numerical accuracy, stability, and convergence, which although deserving careful investigations fall out of the scope of the present paper.

For the important case of hydrogen flow in metal, the present model extends the ones of Krom et al. [6] - which emanates from the previous work of Sofronis and McMeeking [5] - by removing Oriani's assumption of infinitely fast kinetics, Anand and co-workers [65, 41] as well as Toribio and Kharin [8] by extending van't Hoff equation for mass action and introducing mechanical effects. The works of Bower and co-workers [66, 67, 68] on the response of electrode particles in Li-ion batteries, can be recovered from the present model by selecting ad hoc chemical potentials or values for the chemical reaction constants. Different from the inspiring approach of Drozdov [36, 69], the chemical kinetics has been expressed in mass action form, in an appealing thermodynamic framework. McNabb and Foster [1] description of kinetics has not been considered here.

Three case-studies have been discussed in order of complexity and have shown the capability of the present model to reproduce intricate phenomena in different settings. Depending upon the choice of constitutive specifications, the number of material parameters may be significant. In some cases their experimental estimation may be found to be basically impossible. The role of sensitivity analysis and uncertainty quantification, as well as the extension of the present effort to large strains, will be thus very important and carefully considered in further applications of this model to bio- and chemo-mechanics.

The framework illustrated here has been recently used in [70], showing that multi-physics interactions drive Vascular Endothelial Growth Factor Receptor-2 (VEGFR2) relocation on endothelial cells. The relocation of VEGFR2 on the cell membrane during its adhesion to ligand-enriched extra-cellular matrix was described accounting for the ligands-receptors chemical interaction, the diffusion of receptors along the membrane, and the mechanical deformation of the cell. VEGFR2 is recruited by VEGFR2-ligands, which are immobilized on the substrate. Accordingly, the complex that is chemically formed is immobile as well and only a model with "trapping" was able to explain the experimental observation published in [70], which cannot be modeled using conventional treatments.

Acknowledgements

References

[1] A. McNabb and P.K. Foster. A new analysis of the diffusion of hydrogen in iron and ferritic steels. *T METALL SOC AIME*, 227:618–627, 1963.

[2] R.A. Oriani. The diffusion and trapping of hydrogen in steel. *ACTA METALL MATER*, 18(1):147–157, 1970.

[3] J.P. Hirth. Effects of hydrogen on the properties of iron and steel. *METALL TRANS A*, 11A:861–876, 1980.

[4] A.J. Kumnick and H.H Johnson. Deep trapping states for hydrogen in deformed iron. *ACTA METALL MATER*, 28:33–39, 1980.

[5] P. Sofronis and R.M. McMeeking. Numerical analysis of hydrogen transport near a blunting crack tip. *J MECH PHYS SOLIDS*, 37(317-350), 1989.

[6] A.H.M. Krom, R.W.J Koers, and A. Bakker. Hydrogen transport near a blunting crack tip. *J MECH PHYS SOLIDS*, 47:971–992, 1999.

[7] A.H.M. Krom and A. Bakker. Hydrogen trapping models in steel. *METALL MATER TRANS B*, 31B:1475–1482, 2000.

[8] J. Toribio and V. Kharin. A generalised model of hydrogen diffusion in metals with multiple trap types. *PHILOS MAG*, 95(31):3429–3451, 2015.

[9] Q. Zhang and R.E. White. Moving boundary model for the discharge of a $LiCoO_2$ electrode. *J ELECTROCHEM SOC*, 154(6):A587–A596, 2007.

[10] M. Pharr, K. Zhao, X. Wang, Z. Suo, and J.J. Vlassak. Kinetics of initial lithiation of crystalline silicon electrodes of lithium-ion batteries. *NANO LETT*, 12:5039–5047, 2012.

[11] K. Zhao, M. Pharr, Q. Wan, W.L. Wang, E. Kaxiras, J.J. Vlassak, and Z. Suo. Concurrent reaction and plasticity during initial lithiation of crystalline silicon in Lithium-ion batteries. *J ELECTROCHEM SOC*, 159:A238–A243, 2012.

[12] X.H. Liu, J.W. Wang, S. Huang, F. Fan, X. Huang, Y. Liu, S. Krylyuk, J. Yoo, S.A. Dayeh, A.V. Davydov, S.X. Mao, S.T. Picraux, S. Zhang, J. Li, T. Zhu, and J.Y. Huang. In situ atomic-scale imaging of electrochemical lithiation in silicon. *NAT NANOTECHNOL*, 7:749–756, 2012.

[13] M.T. McDowell, S.W. Lee, J.T. Harris, B.A. Korgel, C. Wang, W.D. Nix, and Y. Cui. In situ TEM of two-phase lithiation of amorphous silicon nanospheres. *NANO LETT*, 13(2):758–764, 2013.

[14] J. W. Wang, Y. He, F. Fan, X.H. Liu, S. Xia, Y. Liu, C.T. Harris, H. Li, J.Y. Huang, S.X. Mao, and T. Zhu. Two-phase electrochemical lithiation in amorphous silicon. *NANO LETT*, 13(2):709–715, 2013.

[15] L.B. Freund and Y. Lin. The role of binder mobility in spontaneous adhesive contact and implication for cell adhesion. *J MECH PHYS SOLIDS*, 52:2455–2472, 2004.

[16] V. Deshpande, R.M. McMeeking, and A.G. Evans. A model for the contractility of the cytoskeleton including the effects of stress-fiber formation and dissociation. *P R SOC A*, 463:787–815, 2007.

[17] V. Deshpande, M. Mrksich, R.M. McMeeking, and A.G. Evans. A bio-mechanical model for coupling cell contractility with focal adhesion formation. *J MECH PHYS SOLIDS*, 56:1484–1510, 2008.

[18] W. Ronan, V. Deshpande, R.M. McMeeking, and J.P. McGarry. Cellular contractility and substrate elasticity: a numerical investigation of the actin cytoskeleton and cell adhesion. *BIOMECH MODEL MECHANOBIOL*, 13(417-435), 2014.

[19] S. Torquato. *Random Heterogeneous Materials: Microstructure and Macroscopic Properties*. Springer, 2002.

[20] F. Larche and J.W. Cahn. A linear theory of thermochemical equilibrium under stress. *ACTA METALL MATER*, 21:1051–1063, 1973.

[21] S.R. De Groot and P. Mazur. *Non-Equilibrium Thermodynamics*. Dover, 1984.

[22] R. DeHoff. *Thermodynamic in material science*. CRC Press - Taylor and Francis, 2006.

[23] M.E. Gurtin, E. Fried, and L. Anand. *The Mechanics and Thermodynamics of Continua*. Cambridge University Press, 2010.

[24] E.B. Tadmor, R.E. Miller, and R.S. Elliott. *Continuum Mechanics and Thermodynamics: From Fundamental Concepts to Governing Equations*. Cambridge University Press, 2011.

[25] S. Shell. *Thermodynamics and statistical mechanics: an integrated approach*. Cambridge University Press, 2015.

[26] F. Larche and J.W. Cahn. Non linear theory of thermochemical equilibrium under stress. *ACTA METALL MATER*, 26:53–60, 1978.

[27] G. Holzapfel. *Nonlinear Solid Mechanics: A Continuum Approach for Engineering*. John Wiley & Sons, Ltd., 2001.

[28] S. Paolucci. *Continuum Mechanics and Thermodynamics of Matter*. Cambridge University Press, 2016.

[29] V.A. Lubarda. Consitutive theories based on the multiplicative decomposition of deformation gradient: Thermoelasticity, elastoplasticity, and biomechanics. *APPL MECH REV*, 57(2):95–108, 2004.

[30] J.C. Simo. A framework for finite strain elastoplasticity based on maximum plastic dissipation and the multiplicative decomposition: Part I. Continuum formulation. *COMPUT METHOD APPL M*, 66(2):199 – 219, 1988.

[31] J.C. Simo. A framework for finite strain elastoplasticity based on maximum plastic dissipation and the multiplicative decomposition. Part II: Computational aspects. *COMPUT METHOD APPL M*, 68(1):1 – 31, 1988.

[32] I. Prigogine. Nobel lecture: Time, structure and fluctuations., 1977.

[33] L. Anand. A Cahn-Hilliard-type theory for species diffusion coupled with large elastic-plastic deformations. *J MECH PHYS SOLIDS*, 60(12):1983–2002, 2012.

[34] P. Rosakis, A.J. Rosakis, G. Ravichandran, and J. Hodowany. A thermodynamic internal variable model for the partition of plastic work into heat and stored energy in metals. *J MECH PHYS SOLIDS*, 48:581–607, 2000.

[35] C. Di Leo, E. Rejovitzky, and L. Anand. A Cahn-Hilliard-type phase-field theory for species diffusion coupled with large elastic deformations: Application to phase-separating Li-ion electrode materials. *J MECH PHYS SOLIDS*, 70:1–29, 2014.

[36] A.D. Drozdov. Viscoplastic response of electrode particles in Li-ion batteries driven by insertion of Lithium. *INT J SOLIDS STRUCT*, 51:690–705, 2014.

[37] E. Bohn, T. Eckl, M. Kamlah, and R. McMeeking. A model for Lithium diffusion and stress generation in an intercalation storage particle with phase change. *J ELECTROCHEM SOC*, 160(10):A1638–A1652, 2013.

[38] J. Lemaitre and J.L. Chaboche. *Mechanics of solid materials*. Cambridge University Press, 2000.

[39] K. Hackl and F.D. Fischer. On the relation between the principle of maximum dissipation and inelastic evolution given by dissipation potentials. *P R SOC A*, 464(2089):117–132, 2008.

[40] J.P. Thomas and C.E. Chopin. Modeling of coupled deformation-diffusion in non-porous solids. *INT J ENG SCI*, 37:1–24, 1999.

[41] C. Di Leo and L. Anand. Hydrogen in metals: a coupled theory for species diffusion and large elastic-plastic deformations. *INT J PLASTICITY*, 43:42–69, 2013.

[42] J.C. Simo and T.J.R. Hughes. *Computational inelasticity*. Springer-Verlag, New York, 1998.

[43] A. Villani, E. P. Busso, K. Ammar, S. Forest, and M. G. D. Geers. A fully coupled diffusional-mechanical formulation: numerical implementation, analytical validation, and effects of plasticity on equilibrium. *ARCH APPL MECH*, 84:1647–1664, 2014.

[44] A. Salvadori, D. Grazioli, and M.G.D. Geers. Governing equations for a two-scale analysis of Li-ion battery cells. *INT J SOLIDS STRUCT*, 59:90–109, 2015.

[45] A. Salvadori, E. Bosco, and D. Grazioli. A computational homogenization approach for Li-ion battery cells. Part 1 - Formulation. *J MECH PHYS SOLIDS*, 65:114–137, 2014.

[46] M. Klinsmann, D. Rosato, M. Kamlah, and R.M. McMeeking. Modeling crack growth during Li extraction in storage particles using a fracture phase field approach. *J ELECTROCHEM SOC*, 163(2):A102–A118, 2016.

[47] R.T. Purkayastha and R.M. McMeeking. A linearized model for Lithium ion batteries and maps for their performance and failure. *J APPL MECH*, 79:1–16, 2012.

[48] R.T. Purkayastha and R.M. McMeeking. A parameter study of intercalation of Lithium into storage particles in a Lithium-ion battery. *COMP MATER SCI*, 80:2–14, 2013.

[49] D. Grazioli, M. Magri, and A. Salvadori. Computational modeling of Li-ion batteries. *COMPUT MECH*, 58(6):889–909, 2016.

[50] R.A. Huggins. *Energy storage*. Springer, 2010.

[51] K. Mizushima, P.C. Jones, P.J. Wiseman, and J.B. Goodenough. Li_xCoO_2: A new cathode material for batteries of high energy density. *MRS BULLETIN*, 15(6):783 – 789, 1980.

[52] A. Salvadori, D. Grazioli, M.G.D. Geers, D. Danilov, and P.H.L Notten. A multiscale-compatible approach in modeling ionic transport in the electrolyte of (lithium ion) batteries. *J POWER SOURCES*, 293:892–911, 2015.

[53] A. Salvadori, D. Grazioli, M. Magri, M.G.D. Geers, D. Danilov, and P.H.L. Notten. On the role of saturation in modeling ionic transport in the electrolyte of (Li-ion) batteries. *J POWER SOURCES*, 294:696–710, 2015.

[54] M. Magri. *A theory for the analysis of electro-chemo-mechanical systems and its application to Li-ion batteries*. PhD thesis, University of Brescia, 2018.

[55] V.A. Sethuraman, M.J. Chon, M. Shimshak, V. Srinivasan, and P.R. Guduru. In situ measurements of stress evolution in silicon thin films during electrochemical lithiation and delithiation. *J POWER SOURCES*, 195:5062–5066, 2010.

[56] S. Renganathan, G. Sikha, S. Santhanagopalan, and R. E. White. Theoretical analysis of stresses in a Lithium ion cell. *J ELECTROCHEM SOC*, 157:155–163, 2010.

[57] N. Nitta, F. Wu, J.T. Lee, and G. Yushin. Li-ion battery materials: present and future. *MATER TODAY*, 18(5):252 – 264, 2015.

[58] X.H. Liu, L. Zhong, S. Huang, S.X. Mao, T. Zhu, and J.Y. Huang. Size-dependent fracture of silicon nanoparticles during lithiation. *ACS NANO*, 6:1522–1531, 2012.

[59] A. Mukhopadhyay and B.V. Sheldon. Deformation and stress in electrode materials for Li-ion batteries. *PROG MATER SCI*, 63:58–116, 2014.

[60] E. Bosco, V.G. Kouznetsova, E.W.C. Coenen, M.G.D. Geers, and A. Salvadori. Multiscale computational homogenization-localization modelling of microscale damage towards macroscopic failure: describing non-uniform fields across discontinuity. *COMPUT MECH*, 54:299–319, 2014.

[61] A. Salvadori and A. Carini. Minimum theorems in incremental linear elastic fracture mechanics. *INT J SOLIDS STRUCT*, 48:1362–1369, 2011.

[62] A. Salvadori and F. Fantoni. Minimum theorems in 3D incremental linear elastic fracture mechanics. *INT J FRACTURE*, 184(1):57–74, 2013.

[63] A. Salvadori and F. Fantoni. On a 3D crack tracking algorithm and its variational nature. *J EUR CERAM SOC*, 34:2807–2821, 2014.

[64] A. Salvadori and F. Fantoni. Fracture propagation in brittle materials as a standard dissipative process: general theorems and crack tracking algorithms. *J MECH PHYS SOLIDS*, 95:681–696, 2016.

[65] L. Anand. A thermo-mechanically-coupled theory accounting for hydrogen diffusion and large elastic-viscoplastic deformations of metals. *INT J SOLIDS STRUCT*, 48:962–971, 2011.

[66] A.F. Bower, P.R. Guduru, and E. Chason. A continuum model of deformation, transport and irreversible changes in atomic structure in amorphous Lithium–silicon electrodes. *ACTA MATER*, 98:229–241, 2015.

[67] A.F. Bower, P.M. Guduru, and V.A. Sethuraman. A finite strain model of stress, diffusion, plastic flow and electrochemical reactions in a Lithium-ion half-cell. *J MECH PHYS SOLIDS*, 59:804–828, 2011.

[68] A.F. Bower and P.M. Guduru. A simple finite element model of diffusion, finite deformation, plasticity and fracture in Lithium ion insertion electrode materials. *MODELLING SIMUL MATER SCI ENG*, 20:045004, 2012.

[69] A.D. Drozdov. A model for the mechanical response of electrode particles induced by Lithium diffusion in Li-ion batteries. *ACTA MECH*, 225:2987–3005, 2014.

[70] V. Damioli, A. Salvadori, G.P. Beretta, C. Ravelli, and S. Mitola. Multi-physics interactions drive VEGFR2 relocation on endothelial cells. *SCI REP-UK*, 7(1):16700, 2017.

A J_2 flow theory with isotropic hardening

We assume that: i) the viscous stress is neglected and $\boldsymbol{\sigma}^e$ identifies with Cauchy's stress $\boldsymbol{\sigma}$; ii) only one scalar internal variable ξ is used and

$$\psi_{in}(\xi) = \frac{1}{2} K^{in} \xi^2 \, , \qquad K^{in} \geq 0 \tag{101a}$$

together with a von Mises yield criterion

$$\varphi^{in}(\boldsymbol{\sigma}, \chi) = || \operatorname{dev}[\boldsymbol{\sigma}] || - \sqrt{\frac{2}{3}} \sigma_Y + \chi = 0 \tag{101b}$$

and associated flow rule (58). The term σ_Y in Eq.(101b) denotes the yield stress while χ is a hardening parameter defined by Eq.(27). Kuhn-Tucker conditions

$$\frac{\partial \lambda}{\partial t} \geq 0 \, , \qquad \varphi^{in} \leq 0 \, , \qquad \frac{\partial \lambda}{\partial t} \varphi^{in} = 0 \tag{101c}$$

complete the incremental form of the mechanical constitutive equations.

Owing to definitions (27), (48), and (49) the thermodynamic restriction (31a) is rephrased as follows

$$\boldsymbol{\sigma} : \frac{\partial \boldsymbol{\varepsilon}^{in}}{\partial t} + \chi \frac{\partial \xi}{\partial t} - RT \ln(1 - \theta_T) \frac{\partial c_T^{max}}{\partial \xi} \frac{\partial \xi}{\partial t} \geq 0 \tag{102}$$

In view of normal flow rules (58), the first two terms of (102) can be written as

$$\boldsymbol{\sigma} : \frac{\partial \boldsymbol{\varepsilon}^{in}}{\partial t} + \chi \frac{\partial \xi}{\partial t} \overset{\varphi^{in}=0}{=} (\| \operatorname{dev} [\boldsymbol{\sigma}] \| + \chi) \frac{\partial \lambda}{\partial t} \overset{\varphi^{in}=0}{=} \sqrt{\frac{2}{3}} \sigma_Y \frac{\partial \lambda}{\partial t} \geq 0 \tag{103}$$

with $\lambda \geq 0$ the monotonically increasing plastic multiplier. Restriction (102) is left with

$$- \log(1 - \theta_T) \frac{\partial c_T^{max}}{\partial \xi} \frac{\partial \lambda}{\partial t} \geq 0 \tag{104}$$

The term $\log(1 - \theta_T)$ is always negative since the trap concentration c_T cannot exceed the upper bound set by the saturation limit c_T^{max} and thus $0 \leq \theta_T \leq 1$. In view of experimental observations [4] showing that the number of trap sites increases with plastic deformation the positiveness of $\frac{\partial c_T^{max}}{\partial \xi}$ is guaranteed and therefore thermodynamic consistency (102) prevails.

B Energy balance

Making use of the time derivative of the internal energy (Eq. (13)) and of the thermodynamic prescriptions (29), the energy balance (32) can be written as

$$-T \frac{\mathrm{d}}{\mathrm{d}t} \frac{\partial \psi}{\partial T} = \boldsymbol{\sigma}^d : \frac{\partial \boldsymbol{\varepsilon}^{cte}}{\partial t} + \boldsymbol{\sigma} : \frac{\partial \boldsymbol{\varepsilon}^{in}}{\partial t} + s_q - \operatorname{div}[\vec{q}] + ({}^u\mu_L - \mu_L) \frac{\partial c_L}{\partial t} +$$
$$({}^u\mu_T - \mu_T) \frac{\partial c_T}{\partial t} - \vec{h}_L \cdot \nabla [{}^u\mu_L] + ({}^u\mu_L - {}^u\mu_T) \, w^{(1)} \, . \tag{105}$$

The time derivative of the Helmholtz free energy has been derived in Eq.(26). It holds accordingly:

$$-T \frac{\mathrm{d}}{\mathrm{d}t} \frac{\partial \psi}{\partial T} = -T \frac{\partial^2 \psi}{\partial T^2} \frac{\partial T}{\partial t} - T \frac{\partial^2 \psi}{\partial T \partial \boldsymbol{\varepsilon}^{cte}} : \frac{\partial \boldsymbol{\varepsilon}^{cte}}{\partial t} - T \frac{\partial^2 \psi}{\partial T \partial c_L} \frac{\partial c_L}{\partial t} - T \frac{\partial^2 \psi}{\partial T \partial c_T} \frac{\partial c_T}{\partial t} - T \frac{\partial^2 \psi}{\partial T \partial \boldsymbol{\xi}} : \frac{\partial \boldsymbol{\xi}}{\partial t} \, . \tag{106}$$

If the latter is inserted in (105), the coefficient of $\frac{\partial c_L}{\partial t}$ turns out to be

$$\left(T \frac{\partial^2 \psi}{\partial T \partial c_L} + {}^u\mu_L - \mu_L \right)$$

and vanishes in view of identity (38a) and of the definition (17) of μ_L. The same comes out for the coefficient of $\frac{\partial c_T}{\partial t}$. In summary, the generalized heat equation holds

$$-T \frac{\partial^2 \psi}{\partial T^2} \frac{\partial T}{\partial t} - \operatorname{div}[\boldsymbol{K} \nabla [T]] = s_q + T \frac{\partial^2 \psi}{\partial T \partial \boldsymbol{\varepsilon}^{cte}} : \frac{\partial \boldsymbol{\varepsilon}^{cte}}{\partial t} + T \frac{\partial^2 \psi}{\partial T \partial \boldsymbol{\xi}} : \frac{\partial \boldsymbol{\xi}}{\partial t} + \boldsymbol{\sigma}^d : \frac{\partial \boldsymbol{\varepsilon}^{cte}}{\partial t} +$$
$$+ \boldsymbol{\sigma} : \frac{\partial \boldsymbol{\varepsilon}^{in}}{\partial t} - \vec{h}_L \cdot \nabla [{}^u\mu_L] + ({}^u\mu_L - {}^u\mu_T) \, w^{(1)} \tag{107}$$

with ${}^u\mu_L$ and ${}^u\mu_T$ from Eq. (38b) and $w^{(1)}$ from Eq. (62).